



Contents lists available at ScienceDirect

Journal of Quantitative Spectroscopy & Radiative Transfer

journal homepage: www.elsevier.com/locate/jqsrt

Version 4 retrievals for the atmospheric chemistry experiment Fourier transform spectrometer (ACE-FTS) and imagers

C.D. Boone^{a,*}, P.F. Bernath^{a,b}, D. Cok^a, S.C. Jones^a, J. Steffen^a^a Department of Chemistry, University of Waterloo, 200 University Avenue West, Ontario N2L 3G1, Canada^b Department of Chemistry and Biochemistry, Old Dominion University, Norfolk, VA 23529, United States of America

ARTICLE INFO

Article history:

Received 19 August 2019

Revised 13 February 2020

Accepted 2 March 2020

Available online 3 March 2020

Keywords:

Fourier transform spectroscopy

Remote sensing

Retrievals

ABSTRACT

The Atmospheric Chemistry Experiment is a satellite-based mission that has been probing the Earth's atmosphere via solar occultation since February 2004. Instruments on board include a high resolution Fourier transform spectrometer (ACE-FTS) and a pair of filtered imagers. A new processing version (version 4, with version 4.1 representing the most recent update) has been implemented for these instruments. Analysis for the ACE-FTS instrument makes use of the latest spectroscopic information and features improved accuracy in forward model calculations, including a new instrumental line shape and employing a 100 m altitude sub-grid within the tangent layer of the 1 km altitude grid employed in previous processing versions. Changes were made in the handling of solar and deep space calibration spectra to avoid systematic errors that impacted previous processing versions. Emphasis was placed on improving software robustness, as well as minimizing occurrences of unphysical oscillation in retrieved profiles. Seven new molecules and three new isotopologues were added to the list of atmospheric constituents retrieved from the previous processing version (version 3.5/3.6) for a total of 44 molecules and 24 isotopologues. For the imagers, forward model calculations were changed to a 100 m altitude grid (rather than a 1 km grid) in version 4 processing.

© 2020 Elsevier Ltd. All rights reserved.

1. Introduction

Developed under the auspices of the Canadian Space Agency, the Atmospheric Chemistry Experiment (ACE) is a satellite-based mission for remote sensing of the Earth's atmosphere [1,2]. On board the small science satellite SCISAT, it was launched August 12, 2003 into a circular, highly inclined orbit (650 km altitude, 74° inclination to the equator). The measurement technique employed is solar occultation. Using the Sun as a light source, instruments collect a series of atmospheric absorption measurements as the Sun rises or sets from the orbiting satellite's perspective, providing up to 30 measurement opportunities per day.

The primary instrument on SCISAT is the Atmospheric Chemistry Experiment Fourier transform spectrometer (ACE-FTS), featuring high resolution (± 25 cm maximum optical path difference, 0.02 cm^{-1} resolution), broad spectral coverage in the mid infrared (750 – 4400 cm^{-1}), and a signal-to-noise ratio ranging from just under 100:1 up to ~ 400 :1 [3]. The satellite also includes the Atmospheric Chemistry Experiment Measurement of Aerosol Extinction in the Stratosphere and Troposphere Retrieved by Occultation

(ACE-MAESTRO) instrument [4], a dual diode-array spectrometer measuring in the ultraviolet, visible, and infrared (400–1010 nm) with a spectral resolution of 1.5–2 nm and a signal-to-noise ratio ranging from 1000:1 to 3000:1. There is also a pair of filtered imagers on board [5], each featuring a signal-to-noise ratio of ~ 1500 : a visible imager centered at 527.11 nm with a full width at half maximum bandwidth of 13.28 nm and a near infrared imager centered at 1020.55 nm with bandwidth 19.44 nm.

The main science goal of ACE at launch was “understanding the chemical and dynamical processes that control the distribution of ozone in the stratosphere and upper troposphere, particularly in the Arctic” [1]. The mission had a planned lifetime of 2 years, but with more than 16 years in orbit, ACE data are being used extensively to measure changes in atmospheric composition. More than 450 publications make use of ACE data that covers the atmosphere from 5 km (or the cloud tops) in the troposphere to about 120 km in the lower thermosphere.

The first stable processing version for the ACE-FTS instrument was version 2.2 [6]. Upgrades implemented for versions 3.0 through 3.6 processing are described by Boone et al. in 2013 [7]. This manuscript describes changes applied to the analysis in version 4 (i.e., version 4.0 and the most recent update version 4.1) compared to these previous processing versions. More details on

* Corresponding author.

E-mail address: cboone@scisat.ca (C.D. Boone).

aspects of the processing that have not changed for the current version can be found in the papers describing previous processing versions.

2. Input data sources

Data from the SCISAT satellite are downlinked to various ground stations around the world, collected by the Mission Operations Center (MOC) in St. Hubert, Quebec, and then transferred to the Science Operations Center (SOC) at the University of Waterloo for processing. SCISAT downlinks ~2 GB of raw data each day. With limited onboard memory available (1.5 GB) to store data between ground station contacts, this downlink capacity is sometimes insufficient to permit measurement of all available occultations (a maximum of 15 sunrise and 15 sunset events per day). Occultations are therefore occasionally skipped to avoid overfilling onboard storage, which would result in the loss of all data remaining in memory. The schedule governing which occultations to measure and which ones to skip is generated manually at the SOC, constrained primarily by the allotment of ground station contacts provided by the MOC.

Early in the mission, the set of ground stations consisted of two Canadian facilities and one European station. An additional ground station, the Alaska Satellite Facility, was made available about a year after the mission began. Recently, a number of new ground stations have been added, providing a total of 11 sites for downlinking SCISAT data, including some in the Southern Hemisphere (Chile and Australia) that provide downlink opportunities when Northern Hemisphere sites are not visible from the satellite. With the resulting increased downlink capacity, the frequency of skipped occultations has been greatly reduced compared to early in the mission, but neglecting some occultations to avoid overfilling onboard storage remains a necessary component of SCISAT measurement scheduling.

Data downlinked from SCISAT occasionally suffer losses, for example when desynchronization occurs between the ground station and the satellite during transmission. To maximize the number of occultations measured, no check is made on the fidelity of transmitted data prior to deletion from the satellite. However, downlinks are sometimes 'shadowed,' i.e., recorded by multiple ground stations simultaneously. This permits reconstruction of the original data stream via filling in lost data packets or replacing bad data packets from the downlink recorded by one ground station with good data packets from the shadow downlink recorded by a different ground station. Swapping out bad data packets was not implemented in version 3.6 processing prior to 2016, and so version 4 processing has additional measurements available for that time period, which should serve to improve the analysis for affected occultations (i.e., occultations that were missing one or more measurements in version 3.6 processing which were recovered for version 4 processing).

Below 18 km in version 4 processing, pressure and temperature profiles are fixed to the outputs of the operational global weather assimilation and forecasting system from the Canadian Meteorological Center (see Buehner et al., 2015 [8] and references therein for the evolution of this model over the time frame of the mission). In previous processing versions, some older occultations used information from a regional model rather than the global model, while other occultations employed outputs from forecast runs rather than from global analysis runs, which uses feedback from measurements to improve agreement between model outputs and observations. Other occultations had no information at all. Therefore, pressure and temperature profiles were recalculated for every ACE-FTS occultation, yielding improved internal consistency of this information throughout the mission compared to previous processing versions. It also recovered occultations that had

previously failed to process due to missing or bad input pressure and temperature information.

In pressure/temperature retrievals, the analysis is sensitive to the assumed shapes of the pressure and temperature profiles in the altitude region above the highest analyzed measurement (roughly 125 km). For each occultation, these profiles are calculated from NRLMSISE-00 [9], a global reference atmospheric model developed at the US Naval Research Laboratory. The average mass of atmospheric constituents as a function of altitude calculated from the outputs of this model are also employed in the analysis. Inputs to this model are the solar radio flux at wavelength 10.7 cm ($f_{10.7}$) and the Ap-index, which provides a measure of the average daily level of the Earth's geomagnetic activity. Sources of these data employed in previous processing versions are no longer available, and so a new source was chosen for version 4 processing. Analytical Graphics Inc, which developed the STK (Systems Tool Kit, formerly Satellite Tool Kit) software employed by the ACE mission to calculate the satellite's orbit, provides daily values for both $f_{10.7}$ and the Ap-index on an ftp server [10].

3. Level 0→1 processing

Level 0 refers to interferograms measured by the ACE-FTS instrument. Level 1 refers to atmospheric transmittance spectra, calculated by taking the Fourier transform of the interferograms, subtracting off a self-emission spectrum (the average of a set of spectra measured with the instrument pointed toward deep space) and dividing the atmospheric spectra by an averaged high-sun spectrum (from a set of ACE-FTS solar spectra measured at high altitude, above 160 km, assumed to contain no absorption features from the atmosphere).

While the ACE-FTS instrument typically measures no significant atmospheric absorption for tangent heights above 160 km, there are instances where CO₂ absorption exhibits enhancement in this altitude region, and spectral features from the strong ν_3 band of the molecule persist to extremely high altitude in ACE-FTS measurements, contaminating the set of measurements employed to generate the high sun "reference spectrum" for the occultation. The presence of atmospheric spectral features in the reference spectrum would artificially reduce the apparent strength of ν_3 band CO₂ lines in the calculated atmospheric transmittances.

With no significant source of CO₂ at these altitudes, the enhanced CO₂ absorption near 160 km does not necessarily imply an increase in molecular concentration. The absorption is likely primarily a consequence of non-local thermodynamic equilibrium (non-LTE) effects [11]. The balance between CO and CO₂ may also be playing some role, but the dramatic increase in observed CO₂ signal at high altitude likely results from solar pumping of molecules from excited vibrational states into the ground vibrational state, which yields an enhanced lower state population compared to what one would expect for the given ambient temperature (i.e., a population governed by the Boltzmann distribution). It has not been determined if there is any seasonal and/or geographical relationship in the occurrence of CO₂ absorption in measurements above 160 km.

Fig. 1 shows a portion of the raw ACE-FTS measurements in occultation ss70730 (where "ss" stands for sunset and 70,730 is the number of orbits since launch, a unique identifier for the occultation) for tangent heights between 160 and 180 km, offset along the vertical axis for clarity. There are three CO₂ lines in this wavenumber region, indicated by the arrows. For the lowest measurement in this set (161.6 km), the absorption peaks exceed 2%, and absorption from the lines is evident for tangent heights up to at least 173 km. Averaging in spectra from higher altitudes (not shown in the figure) dilutes the contribution from atmospheric absorption in the reference high sun spectrum, but it is best to avoid con-

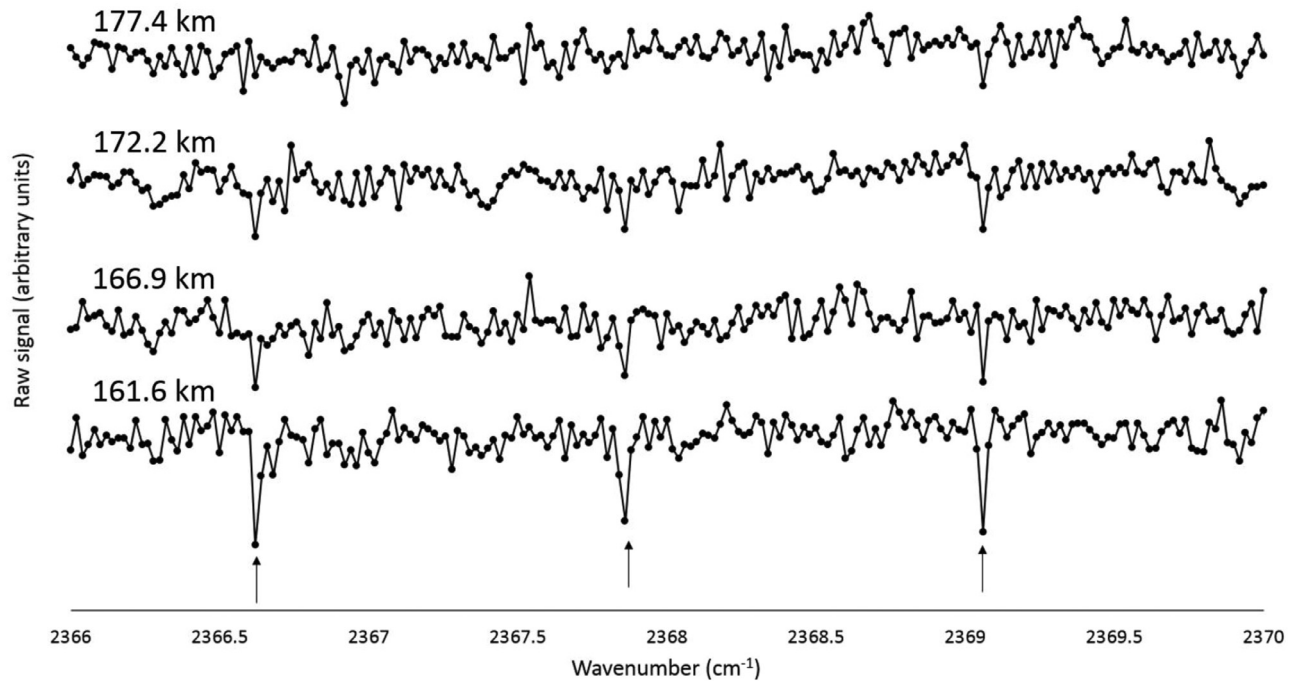


Fig. 1. Measurements between 160 and 180 km in occultation ss70730 containing contributions from atmospheric CO₂. The arrows indicate the locations of CO₂ lines in this wavenumber region. Offsets were applied along the vertical axis to separate the plots for the different tangent heights. For the lowest measurement at 161.6 km, the absorption depth of the CO₂ lines is just over 2%.

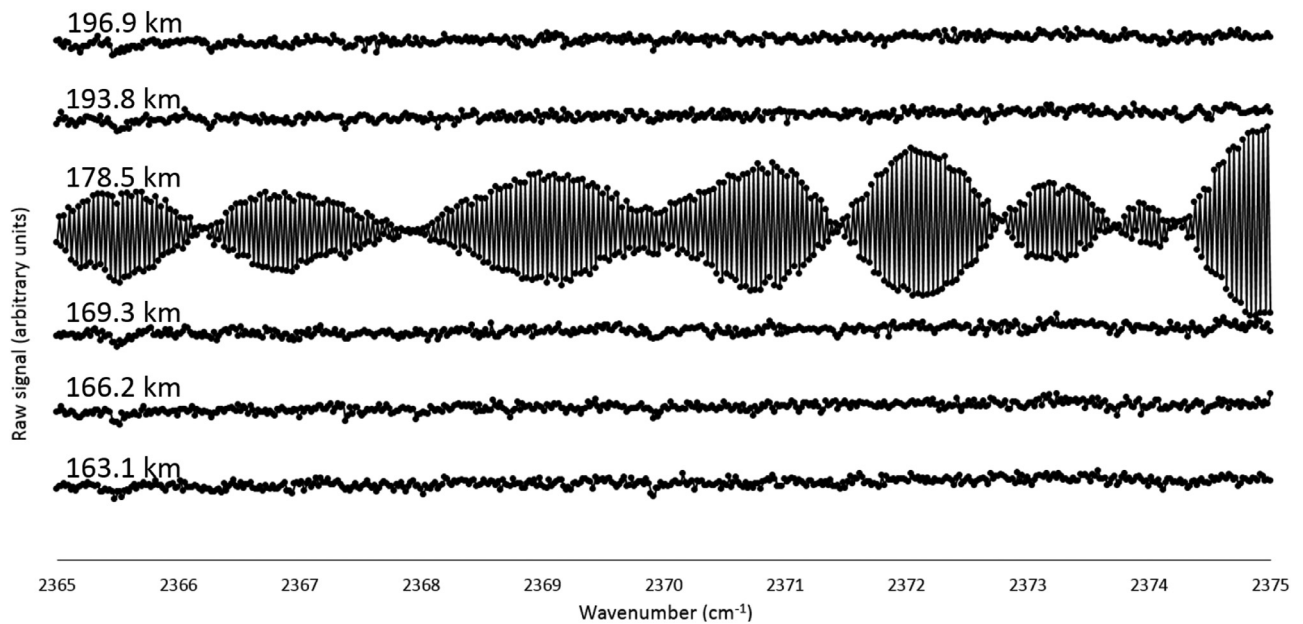


Fig. 2. High sun reference spectra from occultation sr52880. The spectrum for tangent height 178.5 km exhibits large effective noise and is filtered out of ACE-FTS version 4 processing.

tamination of reference spectra altogether. Version 4 processing minimizes this systematic error by identifying spectra that contain contributions from atmospheric CO₂ and excluding these measurements from the calculated average.

On occasion (perhaps once every few dozen occultations), ACE-FTS measurements will encounter problems during calculation of the Fourier transform, typified by a large amplitude beating pattern superimposed on the spectrum. Prior to version 4, checks were made for atmospheric measurements exhibiting large effective noise, which were then excluded from the analysis. However, no such filtering was applied to the deep space and high sun spec-

tra employed in the transmittance calculation. Fig. 2 shows a portion of the high sun calibration spectra measured for occultation sr52880 (where “sr” stands for sunrise). One of the spectra (at tangent height 178.5 km) exhibits a beating pattern. Forward and reverse scans in a given occultation are treated separately, and so this bad high sun spectrum introduced extremely large effective noise into half of the calculated atmospheric transmittance spectra for the occultation, severely impacting the quality of retrievals. For version 4, bad high sun and deep space spectra are identified and removed from the calculated averages for the reference spectra. Bad spectra are identified by calculating the standard deviation

of spectral points in a clean (i.e., free of spectral features) region, looking for situations where the effective noise is above a chosen threshold.

Prior to version 4, transmittance calculations employed reference spectra only from the same occultation as the atmospheric measurements. For a given scan direction, there is a maximum of eight high sun and eight deep space measurements. However, reference spectra vary little over the course of a single day. For version 4, reference spectra of the same occultation type (sunrise or sunset) from within ± 3 orbits are used in the analysis. This provides up to 56 spectra to be included in the average for a given scan direction, reducing noise in the reference spectra and, consequently, the calculated transmittances. It also permits processing of occultations that were missing one or both sets of high sun and deep space reference spectra, where data were lost during downlink to ground stations but most or all of the atmospheric measurements remained available. Several hundred occultations were recovered over the span of the mission through allowing reference spectra to come from different occultations.

The “native” ACE-FTS wavenumber grid is 0.02 cm^{-1} . The wavenumber output of the metrology laser varies with temperature, yielding slightly different spectral sampling in different measurements, and so an interpolation approach must be used to cast ACE-FTS measurements onto this standard grid. Because we calculate the ratio of atmospheric measurements and high sun measurements, we must ensure that all measurements share a common grid.

Previous processing versions performed the interpolation with a 128-point apodized sinc function [12]. Apodization permitted the use of fewer points in the interpolation kernel, providing a relatively rapid calculation at the expense of a loss of accuracy in some wavenumber ranges under certain conditions. The interpolation technique worked very well for wavenumbers where target grid points (in the interpolated spectrum) were near grid points in the original spectrum, or where the spectrum was relatively featureless. Degraded accuracy occurred for wavenumbers where target grid points were far from grid points in the original spectrum (e.g., a target grid point was halfway between two grid points in the original spectrum). In the vicinity of significant spectral structure (e.g., regions with large numbers of O_3 lines), these errors were magnified, often becoming larger than the noise level. For version 4, spectral resampling in $0 \rightarrow 1$ processing employs a 720 point unapodized sinc interpolation, placing greater emphasis on interpolation accuracy than previous processing versions at the expense of longer processing times. Even in regions with high spectral structure, the new interpolation approach yields errors well below the noise level.

4. Level 1 \rightarrow 2 processing

Level 2 refers to altitude profiles for pressure, temperature, and the volume mixing ratios (VMRs) of gaseous atmospheric constituents.

The basic approach for retrieving pressure, temperature, and VMR profiles has been described in previous publications [6,7]. Please refer to these papers for more details, but a brief description will be provided in the following three paragraphs.

For a given occultation event, pressure, temperature, and instrument pointing are determined first. An assumed CO_2 VMR profile is employed up to ~ 60 km, and main isotopologue CO_2 lines are analyzed to derive information on the atmospheric state. The pressure/temperature analysis is split into two altitude regions. Above ~ 50 km, relative instrument pointing information is accurately known from knowledge of the satellite orbit, which permits the propagation of calculated pressure from the equation for hydrostatic equilibrium (using the fitted temperature profile), while

an empirical function is employed to describe the CO_2 VMR profile above ~ 60 km [7]. Below ~ 50 km, refraction and aerosols degrade instrument pointing knowledge, and therefore pointing information (i.e., measurement tangent heights) must be determined from analysis of the spectra. In this low altitude region, with CO_2 fixed to an assumed profile, pressure and temperature are fitted, and the altitude separations between measurement tangent heights are generated using the equation for hydrostatic equilibrium [7]. After pressure, temperature, and pointing are determined, VMR retrievals can then proceed with these quantities fixed in the analysis.

The retrieval for each target atmospheric constituent employs a preselected set of microwindows: narrow wavenumber regions over a particular altitude range that contain spectral features from the target. A global analysis type approach [13] is employed, fitting all data simultaneously using Levenberg-Marquardt least squares fitting [14]. VMR profiles for all contributing molecules in a given microwindow set are fitted simultaneously, with separate VMR profiles employed for different isotopologues of a given molecule, but information on interferers (i.e., everything but the target constituent in the retrieval) is discarded.

Fitted quantities are determined on an altitude grid defined by the measurement tangent heights and interpolated onto a standard altitude grid for forward model calculations. Aerosol (e.g., cloud) contributions to the spectrum not included in the calculated spectrum are accounted for by fitting two “baseline adjustment” parameters in each microwindow segment: a baseline scaling factor and a baseline slope. Optimal estimation is not employed in the analysis. No smoothing constraints are applied. Forward model calculations employ a single ray in the center of the ACE-FTS field of view. A future processing version will implement a modeling of the instrument's field of view (circular with diameter 1.25 mrad, subtending 3–4 km at the tangent point) in the calculation.

The line list for version 4 processing is based primarily on HITRAN 2016 [15], with the addition of $^{15}\text{NO}_2$ from a study by Perrin et al. [16] and COCIF from a study by Perrin et al. [17], neither of which was available in the HITRAN compilation.

A new representation of the ACE-FTS instrumental line shape (ILS) was derived for version 4 [18], providing improved characterization of instrumental effects in calculated spectra compared to previous processing versions. Asymmetry in the ILS is now incorporated into the calculation, and the wavenumber variation of the ILS was modeled better than was achieved with version 3 processing.

4.1. Tangent layer sub-grid

Forward model calculations trace the path of a solar ray as it traverses the atmosphere and integrate absorption experienced along the way. To discretize the integration for ACE-FTS processing, the atmosphere is divided into 150 concentric layers of thickness 1 km, and the calculated absorption coefficient becomes the sum of contributions from all layers the solar ray passes through. Other than the tangent layer (the layer closest to the surface), solar rays encounter each layer twice when transiting the atmosphere. ACE-FTS measurements provide no information on line-of-sight variations, and so a symmetric atmosphere is assumed.

Quantities (pressure, temperature, and VMRs) are assumed constant within a given layer, a convenient simplification of the inhomogeneous vertical atmospheric structure in order to expedite calculations. These values represent the average quantity encountered by a solar ray as it passes through the altitude region in the atmosphere represented by the layer in the calculation grid. However, calculation accuracy suffers in the tangent layer, especially when the solar ray does not fully traverse the layer. For example, when the solar ray associated with a particular measure-

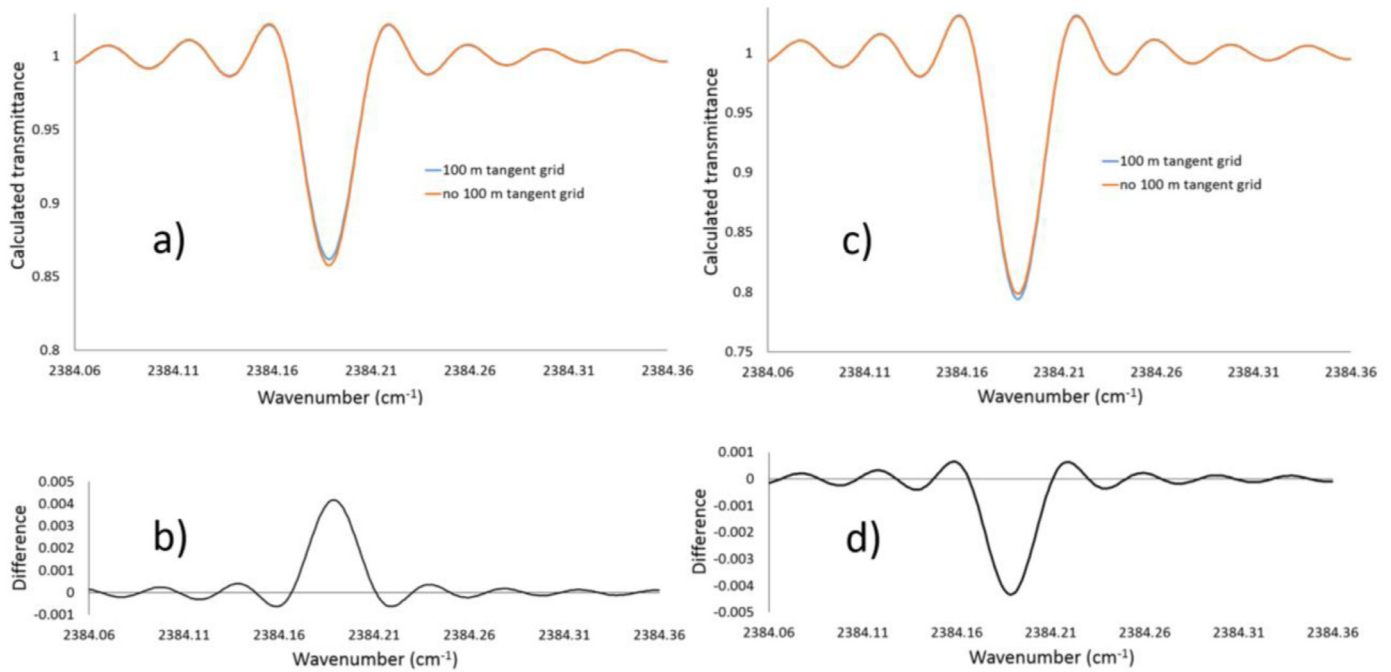


Fig. 3. a) Calculated CO₂ line at 83.76 km in sr10063 with and without a 100 m grid in the tangent layer. b) The difference between the two calculations in panel a. c) Calculated CO₂ line at 82.02 km in sr10063 with and without the 100 m grid in the tangent layer. d) The difference between the two calculations in panel c.

ment skims through the top of the tangent layer, the average pressure in this layer is not representative of what the solar ray experienced in the atmosphere. Forward model calculations often reduce this error by introducing the Curtis-Godson approximation [19] into the calculation, in which the optical thickness for a solar ray passing through a particular grid layer is calculated using VMR-weighted mean values for pressure and temperature along the ray path (rather than the average values in the center of the calculation grid layer). The calculation involves a numerical integration along the inhomogeneous paths of pressure and temperature, performed in conjunction with the ray tracing through the refracting atmosphere [20]. Unfortunately, this approach could complicate the determination of measurement tangent heights at low altitude during the pressure/temperature analysis, and so an alternate approach is used to improve calculation accuracy in the tangent layer, using a relatively simple modification to the grid structure.

Calculation accuracy can be improved by subdividing the 1 km tangent layer into a finer altitude grid having 10 layers of thickness 100 m. The contribution from the tangent layer is then calculated from this finer grid, while contributions from all higher altitude layers are calculated on the normal 1 km grid. This approach has been implemented in forward model calculations for version 4 processing. Fig. 3 shows the differences that can arise from this approach. For a measurement near the top of one of the layers on the 1 km grid (at tangent height 83.76 km in Fig. 3a), a smaller absorption is calculated for the line due to a smaller contribution from the tangent layer. The difference (shown in Fig. 3b) is over 2% at the absorption peak, well above the noise level of the ACE-FTS instrument at the wavenumber for this line. Conversely, for a measurement near the bottom of a layer on the 1 km grid (at tangent height 82.02 km in Fig. 3c), the calculated absorption with the 100 m grid in the tangent layer is over 2% larger at the peak due to an increased contribution from the tangent layer.

Performing the forward model integration via a simple sum of contributions on the 1 km grid clearly leads to a calculation error that depends on the location of the tangent height within the tangent layer for a given measurement, which could induce or en-

hance unphysical oscillations in retrieved profiles. Using the 100 m grid within the tangent layer in ACE-FTS version 4 processing promotes reduced variability compared to previous processing versions.

4.2. Low altitude tangent heights from the N₂ continuum (version 4.1)

Below 18 km, tangent heights in version 4 are generated through analysis of the N₂ collision induced absorption continuum near 2500 cm⁻¹ [21], with pressure and temperature profiles fixed to the output of a model administered by the Canadian weather service (as mentioned previously). Previous processing versions determined tangent heights below 15 km through fitting a set of ¹⁸OCO lines, applying a scaling factor to the CO₂ VMR profile to account for isotopic fractionation and possible systematic errors in the line strengths. Using the N₂ continuum to generate tangent heights permits the retrieval of CO₂ VMR profiles below 18 km in version 4 [22], which was not possible in previous processing versions because an assumed CO₂ VMR profile was employed in deriving tangent heights.

The N₂ continuum analysis in processing version 4.0 [21] fitted for a baseline scaling factor to account for aerosol contributions to the spectrum not included in the calculation. Attempts to include a “baseline slope” term, to account for wavenumber variation in the aerosol contribution through the N₂ continuum region, yielded inconsistencies between retrieved tangent heights and the expectations from CO₂, and so no baseline slope term was employed in the analysis. Under normal conditions, aerosol spectral response in the N₂ continuum region appears to be quite flat, and a simple scaling of the baseline is sufficient to account for aerosol contributions missing in the calculation. However, occultations showing strong polar stratospheric cloud (PSC) signatures [23] can exhibit a significant slope in the spectral response through this wavenumber region, which introduces a large systematic error in the retrieved tangent height. Consequently, in ACE-FTS version 4.0 results, occultations containing strong PSC signatures often exhibit large spikes

in the VMR profiles for all molecules near 18 km. Care should be taken when using results from this processing version for occultations in polar spring, where PSCs might occur.

The primary purpose of version 4.1 was to improve on the N_2 continuum analysis, allowing for the inclusion of a baseline slope term in the fitting, thereby reducing systematic errors for occultations containing PSC signatures in the spectra. Two adjustments were made in the analysis to accomplish this goal. The first adjustment was using non-Voigt line shapes for N_2O and CH_4 lines in the N_2 continuum region. The second adjustment was including far wing contributions from the nearby ν_3 CO_2 band in the calculation rather than trying to avoid CO_2 far wing effects in the microwindow selection process. Including CO_2 far wing effects in the analysis allowed for the extension of microwindows to significantly lower wavenumber, into a region where the N_2 continuum absorption is stronger. The combination of stronger N_2 continuum absorption and the broader wavenumber span of the microwindow set allows for improved differentiation between the N_2 continuum absorption signal and aerosol extinction.

Version 4.1 also employed a set of pseudolines [24] to calculate the HNO_3 contribution in this wavenumber region rather than using a scaled set of residuals derived from ACE-FTS spectra, as was done in version 4.0.

4.2.1. Non Voigt line parameters for the N_2 continuum analysis in version 4.1

The spectroscopic line parameters from HITRAN 2016, the basis for the ACE-FTS version 4 line list, all assume a basic Voigt line shape. A Voigt line shape is generally sufficiently accurate for the analysis of spectral features in ACE-FTS measurements, but there are instances where this is not the case.

One molecule that exhibits particular problems is H_2O in the troposphere [25]. This molecule is known to deviate significantly from a Voigt line shape under pressure conditions found in the troposphere [26], but the large residuals encountered when analyzing H_2O lines in ACE-FTS spectra are often beyond those expectations, enhanced by deficiencies in the forward model calculation approach and by the high variability of tropospheric H_2O . The VMR profile of H_2O changes rapidly as a function of altitude in the troposphere, and using a single ray in the center of the field of view in the forward model calculation (rather than averaging multiple rays across the field of view) makes it difficult to model this altitude variation properly. The 1 km altitude grid can also cause problems, being too coarse to completely capture the altitude variation (H_2O VMR can sometimes change by a factor of two over the span of 1 km in altitude), although the 100 m altitude grid within the tangent grid introduced in version 4 helps in that regard.

The situation is further complicated by the fact that over the course of a single measurement, as the satellite proceeds in its orbit, the pointing of the instrument changes in altitude, thereby “smearing” the measurement across an altitude region where the VMR for the molecule is changing rapidly. The high variability of tropospheric H_2O also serves to enhance the residuals. H_2O can vary significantly along the line of sight, and the geographic location of the tangent point moves over the course of the set of measurements collected during an occultation, both of which can make it difficult to model H_2O lines with a single VMR profile (used for all measurements simultaneously) where the forward model calculation assumes spherical symmetry.

Note that these problems with H_2O only occur in the troposphere; they do not persist into the stratosphere where the molecule exhibits less variability along the line of sight and the VMR profile changes less rapidly with altitude. During microwindow selection for molecules besides H_2O itself, it is routine to avoid (wherever possible) H_2O lines for microwindows that extend

into the troposphere, to avoid getting large systematic residuals that might introduce a bias in the least squares fitting.

Lines from molecules other than H_2O sometimes exhibit systematic residuals when using the Voigt parameters from HITRAN 2016. When these molecules are well mixed, with low variability along the line of sight and a VMR profile that does not change rapidly with altitude, the systematic residuals arise from limitations inherent in the Voigt line shape, unlike H_2O where the residuals arise from a combination of non-Voigt effects in the line shape and other factors. In the N_2 continuum analysis region (2420–2700 cm^{-1}), lines from both N_2O and CH_4 exhibit systematic residuals that indicate something beyond the Voigt line shape is required to properly characterize them.

To reduce systematic residuals in the N_2 continuum region, non-Voigt parameters were generated for CH_4 and N_2O in this wavenumber region from fitting ACE-FTS spectra. Different lines required different line shapes. All of the N_2O lines in the region used a quadratic speed dependent Voigt (qSDV) line shape [25]. For CH_4 , some lines used Voigt with line mixing, some used qSDV without line mixing, while other lines used qSDV with line mixing (qSDVLM) [27], depending on which line shape yielded the best residuals in the analysis of ACE-FTS spectra. It is difficult to determine temperature dependences from ACE-FTS measurements, and so the temperature dependence is fixed in the analysis. The pressure broadening (Γ_0), speed dependence of the pressure broadening (Γ_2), and Rosenkranz first order line mixing (Y) [28] parameters are all assigned the following form for pressure (P) and temperature (T) dependence

$$\chi(P, T) = \chi_0 * P * \left(\frac{296}{T}\right)^n, \quad (1)$$

where 296 K is the typical HITRAN reference temperature, and the temperature exponent n , assumed to be the same for all three parameters, is taken as the value from HITRAN 2016 for the line. Using the functional form in Eq. (1) for line mixing (Y) is a matter of convenience rather than an expectation for the physical nature of the temperature dependence.

The pressure shift (η_0) and speed dependence of the pressure shift (η_2) are both assumed proportional to pressure with no temperature dependence.

Fig. 4 shows the effect on the residuals of including non-Voigt parameters. Fig. 4a shows the calculated contributions to this window for a tangent height near 10 km. There are five relatively strong lines (three main isotopologue N_2O lines and two main isotopologue CH_4), along with an assortment of weaker lines from various isotopologues. Fig. 4b shows the fitting residuals (observed – calculated) from this window for occultation sr10063. The altitude region covered in the analysis was 8–30 km, yielding a total of 33 measurements in the fitting. Residuals for all of the measurements were plotted simultaneously to emphasize systematic features. The five strong lines and one of the weaker CH_4 lines in the window all have large (i.e., well above the measurement noise) systematic features in the residuals that arise from the limitations of using Voigt line shapes in the calculated spectra.

Fig. 4c shows the residuals achieved when using non-Voigt parameters for selected CH_4 and N_2O lines in the calculated spectra. Residuals for three CH_4 lines go to the noise level using a Voigt with line mixing line shape, fitting for three parameters per line (pressure broadening, pressure shift, and line mixing). Using qSDV for N_2O greatly improves the residuals for these lines, but there remain systematic features in the residuals above the noise level. A more complicated line shape might yield residuals closer to the noise level, but since the purpose of the exercise was to improve the N_2 continuum analysis (and not the study of N_2O itself), the level of systematic residuals for the N_2O lines in Fig. 4c was deemed adequate to proceed.

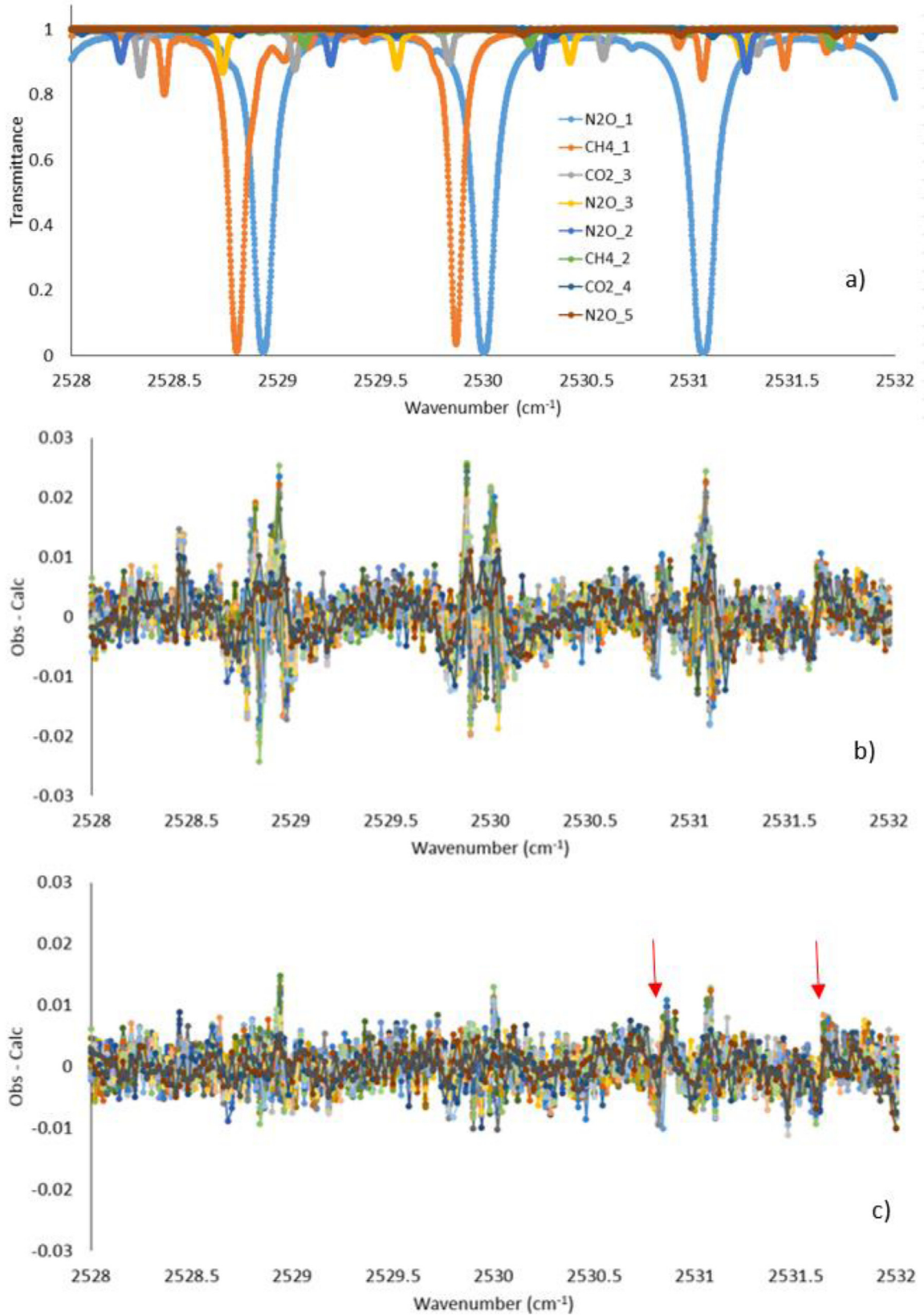


Fig. 4. Effect on fitting residuals from including non-Voigt parameters in the line shapes for CH_4 and N_2O : a) calculated contributions to this region for a tangent height near 10 km (labels indicate molecule name and isotopologue number); b) residuals (observed - calculated) for all measurements between 8 and 30 km (a total of 33 measurements for the given occultation) plotted simultaneously, with the calculated spectra using Voigt parameters from HITRAN 2016; c) the same as b, but using non-Voigt parameters in calculated spectra. Arrows indicate incompletely canceled solar features in the residuals.

The non-Voigt line parameters generated from ACE-FTS spectra for CH₄ and N₂O lines in the N₂ continuum region are provided in a supplemental file to this article (ACEFTS_v4.1_nonVoigt.txt). All spectroscopic parameters not included in the file (line position, line strength, lower state energy, temperature exponent, etc.) were taken from HITRAN 2016. These line parameters are primarily intended to minimize the residuals for the N₂ continuum analysis, although some of the lines using non-Voigt parameters also factor into the retrievals of CH₄ itself. It is not recommended to employ these parameters for conditions outside the range of pressures and temperatures found in the altitude region from the mid troposphere to the mid stratosphere.

It should be noted that the combination of qSDV with line mixing presents some danger of confusion in the sign of the line mixing parameter, based on previously distributed software for calculating qSDVLM. A line profile with Rosenkranz first order line mixing included (g_{LM}) can be expressed in the following form:

$$g_{LM} = \frac{\sqrt{\ln 2/\pi}}{D} \text{Re}[(1 - iY)W(x, y)], \quad (2)$$

where γ_D is the Doppler width, Y is the Rosenkranz line mixing parameter, x is a parameter proportional to the distance from line center, y is a parameter proportional to the width of the line, and $W(x, y)$ is a complex probability function that defines the shape of the line (e.g., Voigt or speed dependent Voigt).

Previous derivations of qSDV in Boone et al. 2008 [25] and the original form of qSDV provided along with the Hartmann-Tran profile (HTP) [29] employed a Fourier transform involving a term of the form $\exp[-i\omega t]$. This form is perfectly valid, but it was pointed out [30] that it would give rise to an expression for line mixing of the following form:

$$g_{LM} = \frac{\sqrt{\ln 2/\pi}}{D} \text{Re}[(1 + iY)W(x, y)], \quad (3)$$

where the sign of the line mixing term is opposite to the normally assumed form in Eq. (2). A revised version of the HTP (and the associated subsidiary profiles such as speed dependent Voigt) was generated using $\exp[+i\omega t]$ [31], which yielded line mixing that followed Eq. (2), making the phase of the line mixing effect consistent with the standard convention employed for Voigt with line mixing.

Thus, for lines with a combination of speed dependence and line mixing (Γ_2 and Y both non-zero), the signs of the Y values provided in the supplemental file would be wrong if using unaltered the subroutine for qSDVLM calculations provided with the Boone et al. paper [27] or the functionally identical qSDVLM subroutine provided along with the original formulation of HTP [29]. The signs reported in the supplemental file would be correct if using an approach that follows the form for line mixing in Eq. (2), such as the subroutine for qSDVLM calculation provided along with the revised formulation of the HTP [31]. For lines in the attached file having the line shape ‘‘Voigt with line mixing’’ ($\Gamma_2 = 0$ and Y non-zero), there is no ambiguity for the sign of Y in the literature.

4.2.2. CO₂ far wing contributions in the N₂ continuum analysis in version 4.1

Far wing absorption from lines in the strong CO₂ ν_3 band extends into the wavenumber region containing the N₂ continuum spectral feature. However, the sub-Lorentzian nature of these lines in the far wing complicate the calculation of their contribution. In version 4.0, this contribution was ignored, and the microwindow set was selected such that the contribution was hopefully minimal.

Fig. 5 shows the calculated CO₂ far wing absorption for a measurement near 10 km tangent height using the tabulated absorption coefficients provided in Cousin et al. [32]. The vertical line in this figure indicates the lower wavenumber limit of microwindows

employed in the N₂ continuum analysis in version 4.0. CO₂ far wing absorption at this altitude was as high as 4% in some version 4.0 microwindows, indicating that ignoring CO₂ far wing contributions in the analysis was inappropriate. Note that the tabulated CO₂ far wing absorption coefficients extend up to 2525 cm⁻¹. Setting the absorption to zero above this point would impart a step in the calculated contribution, and so CO₂ far wing absorption is extrapolated above 2525 cm⁻¹ using a linear function of the natural log of the calculated absorption coefficient between 2500 and 2525 cm⁻¹ for a given measurement.

In order to include this contribution in the version 4.1 N₂ continuum analysis, the microwindow set was pushed to lower wavenumber, into the region of stronger CO₂ far wing absorption. A benefit of this is that the N₂ continuum also has stronger absorption in this wavenumber region. The new version 4.1 microwindow set is presented in Table A1 in the Appendix. The ‘‘Not Fit’’ column refers to the lower wavenumber portion of a window for which the weighting is set to zero in the least squares fitting. Because the wavenumber scale for the ACE-FTS instrument is not fixed, measured and calculated spectra within a given microwindow are automatically aligned prior to analysis, which requires sufficient spectral structure in the window (e.g., a line or a set of lines) to get reasonable information from a cross correlation in wavenumber. Even after generating non-Voigt parameters for lines in this wavenumber region, a number of lines still have systematic residuals, as with the N₂O lines in Fig. 4c. Having a portion of a microwindow with zero weighting in the least squares analysis allows selection of microwindows with sufficient spectral structure to properly align measured and calculated spectra, while avoiding systematic residuals from the window that might negatively influence the least squares fitting results. This approach permitted filling in of large wavenumber gaps that would have otherwise existed in the microwindow set, providing a stronger discrimination between the fitted baseline slope (aerosol contributions) and the N₂ continuum signal.

4.2.3. Version 4.1 N₂ continuum results with a polar stratospheric cloud

In the N₂ continuum analysis, it was found that a separate CO₂ VMR profile had to be used for the CO₂ far wing contribution and CO₂ lines in the region. The fitted VMR for the far wing contribution was typically 15–20% larger. The wavenumber region containing the CO₂ far wing contribution becomes strongly saturated below ~12 km, a consequence of N₂ continuum absorption in the region increasing rapidly with decreasing altitude. Thus, a separate CO₂ VMR is fitted for the line and far wing contributions above 12 km, while a single, common VMR is fitted for the two contributions below 12 km. Otherwise, the fitted VMR for CO₂ far wing would tend to unphysical values (large and negative) below ~8 km, attempting to minimize a small systematic positive bias in the residuals near 2525 cm⁻¹ rather than characterizing the CO₂ far wing contribution in a wavenumber region close to complete saturation at these low altitudes.

With the adjustments applied in the version 4.1 N₂ continuum analysis (non-Voigt spectroscopic parameters, CO₂ far wing contributions, a more robust calculation for the HNO₃ contribution, and smaller wavenumber gaps in the microwindow set relative to version 4.0), it became possible to include a baseline slope term in the analysis while maintaining consistency with expectations from CO₂: i.e., avoiding a step in the results near 18 km, the boundary between the altitude region where tangent heights are generated from the N₂ continuum and tangent height separations are determined from the analysis of CO₂ lines.

Note that, for the microwindow set in Table A1, a common set of baseline scaling and baseline slope terms are used for all mi-

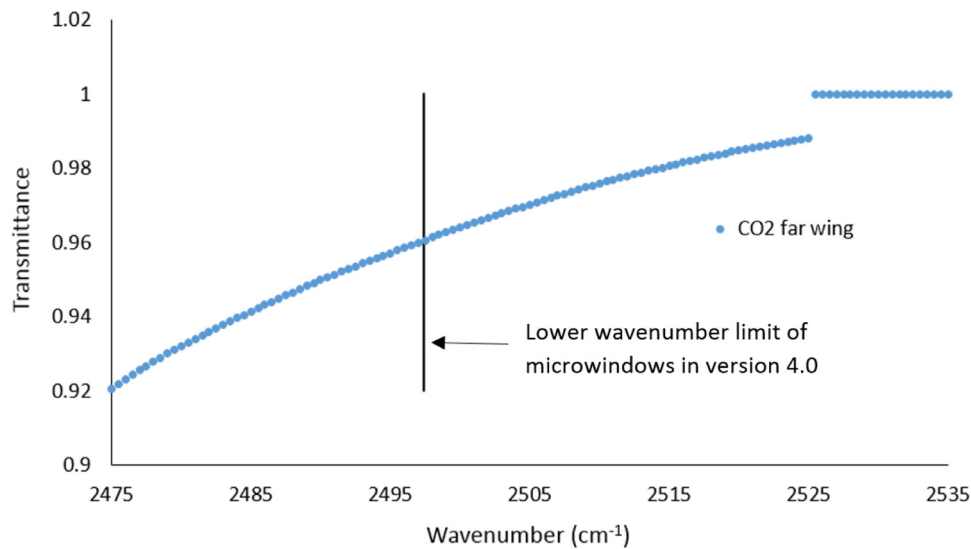


Fig. 5. For a measurement with a tangent height of ~ 10 km, the calculated CO_2 far wing transmittance signal in the vicinity of the lower wavenumber limit (indicated by the vertical line) of the microwindow set employed in N_2 continuum analysis of ACE-FTS version 4.0 processing.

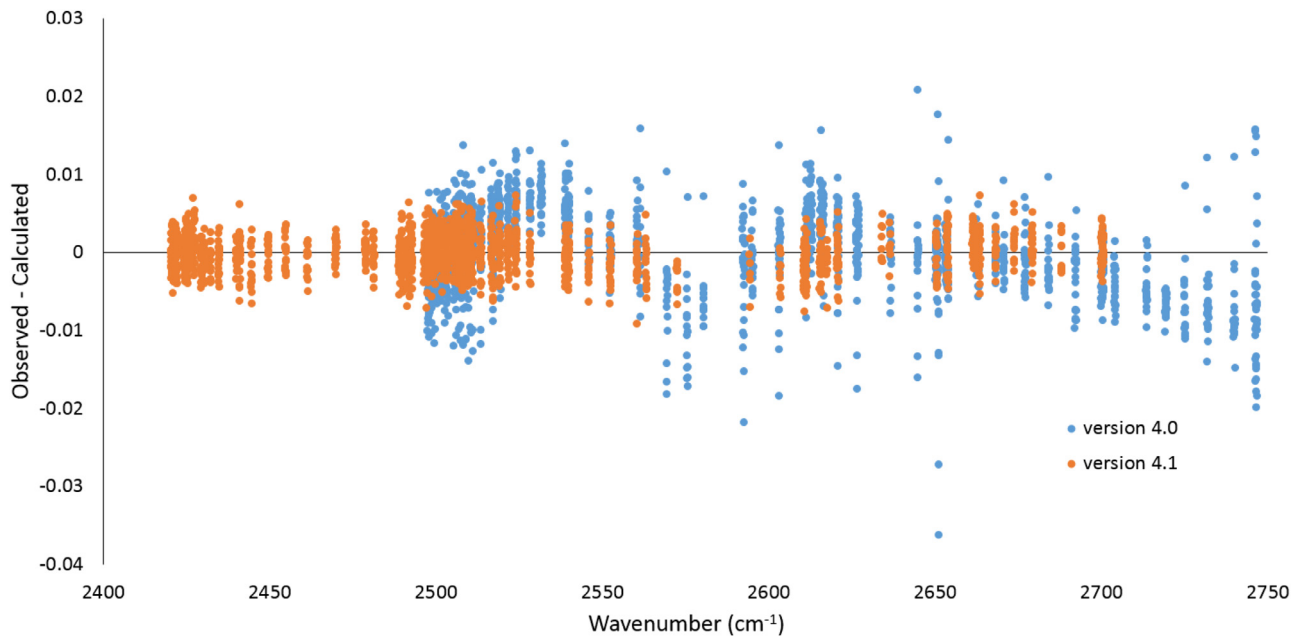


Fig. 6. Fitting residuals from two ACE-FTS processing versions (4.0 in blue and 4.1 in orange) from a measurement near 15.2 km in sr75379 (collected August 10, 2017 at tangent latitude 67.8°S), which is looking through a polar stratospheric cloud. (For interpretation of the references to color in this figure legend, the reader is referred to the web version of this article.)

crowndows excluding those indicated as being “outside windows,” which are microwindows used to improve the information content for particular interferers. These outside windows employ their own baseline terms (scaling and slope) in the analysis.

The inclusion of a baseline slope term permits much improved characterization of aerosols in the N_2 continuum region. For occultations containing the spectral signature of a PSC, the improvement is often dramatic compared to version 4.0. Fig. 6 shows fitting residuals from the N_2 continuum analysis for the two processing versions (4.0 and 4.1) for a measurement with a PSC in the field of view. The residuals corresponding to version 4.1 are significantly better, due in part to the use of non-Voigt parameters for N_2O and CH_4 in this wavenumber region, as well as the baseline slope term accounting for the wavenumber variation of

the PSC spectral signature in the region. In version 4.0, the tangent height determined for this measurement was in error by an enormous amount (~ 2.4 km). For occultations such as this, large errors in tangent heights determined from the N_2 continuum led to spikes in the retrieved VMR profiles of every molecule for the occultation, a consequence of a mismatch with the altitude region above 18 km, which used CO_2 lines in the analysis and was not impacted by the presence of PSCs.

4.3. Pressure/Temperature retrievals

As mentioned previously, Level 1 \rightarrow 2 processing begins with the retrieval of pressure and temperature profiles, along with determining geometry (i.e., tangent heights) for all measurements. The

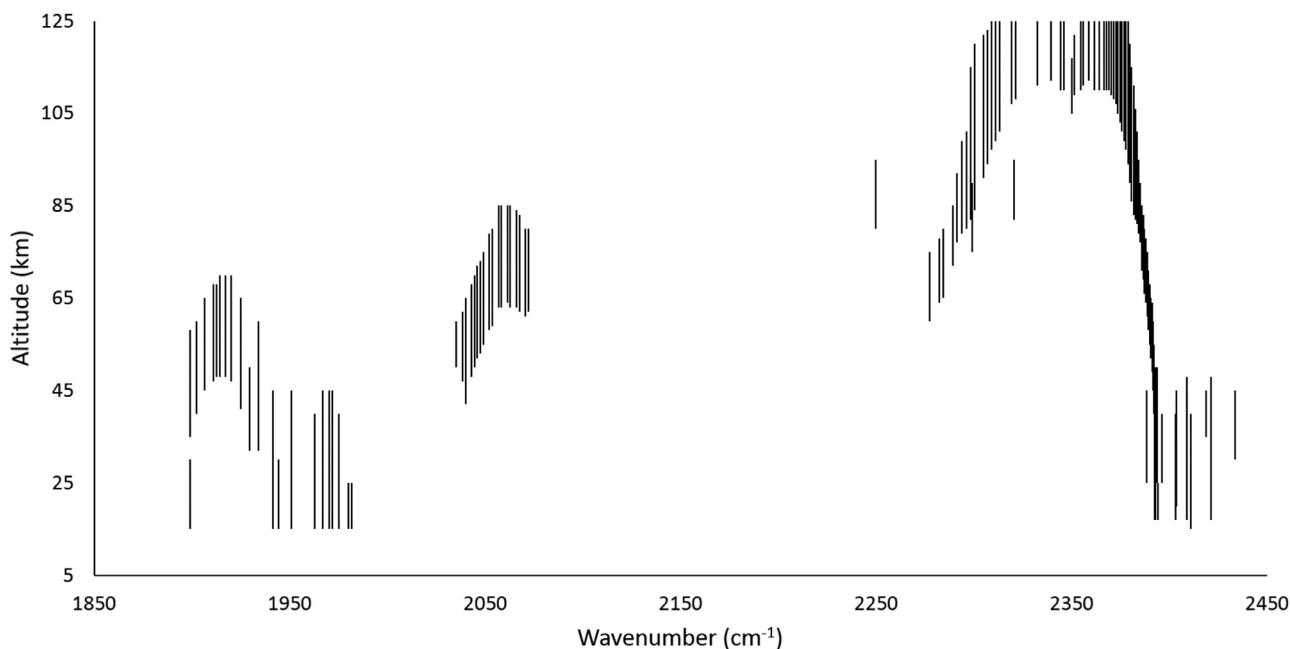


Fig. 7. Graphical depiction of the microwindow set employed in ACE-FTS version 4.1 pressure and temperature retrievals. The location of a line indicates the central wavenumber of a microwindow, while the vertical extent of the line shows the altitude range.

set of microwindows employed in version 4.1 pressure/temperature (P/T) analysis is displayed graphically in Fig. 7 and presented in Table A2 in the appendix. The microwindows for processing version 4.0 (not reported here) attempted to use larger altitude ranges for most microwindows by pushing the analysis to include lower altitudes (greater absorption) in a given window. However, the internal consistency of results degrades significantly when a spectral feature in the “infinite resolution spectrum” (i.e., the calculated spectrum before the convolution with the instrumental line shape) experiences saturation near line center. When saturation occurs, calculated lines exhibit reduced sensitivity to changes in temperature and pressure, and the calculation depends more strongly on the assumed spectral line shape in the wings, which could be less reliable than the knowledge of line shape near line center (Voigt line shapes are assumed for all CO₂ lines employed in the pressure/temperature retrieval). The version 4.1 microwindow set in Table A2 strictly avoids saturation in the calculated infinite resolution spectrum.

Processing versions prior to version 4 used only lines from main isotopologue CO₂, but the microwindow set in Table A2 contains spectral contributions from interferers (subsidiary isotopologues of CO₂, as well as O₃, COF₂, and N₂ quadrupole lines). Strictly avoiding interferers in previous processing versions imposed a significant restriction on the microwindow set, limiting the number of CO₂ main isotopologue lines that could be included in the analysis. Allowing interferers in version 4 alleviates this restriction, adding more CO₂ main isotopologue lines (or larger altitude ranges for some lines) to the analysis.

Unlike previous processing versions, the upper altitude limit for a given microwindow is not strictly defined in version 4 P/T analysis. The software automatically detects the altitude at which a particular CO₂ line drops below the noise level of the instrument and adjusts the upper altitude limit of the microwindow accordingly. This allows for a fuller use of available data while avoiding situations of “fitting noise” for occultations where a particular microwindow extends to altitudes where the signal in the window is below the noise level. Although fitting noise is not a problem in itself (so long as one or more microwindows contain real signal

at the given altitude), the process of aligning the measured and calculated spectra within a window (because the wavenumber calibration of the ACE-FTS instrument is not fixed) could shift the calculated line into alignment with the largest nearby noise feature in the measurement, which might introduce a bias.

As with previous processing versions, the P/T analysis is separated into two altitude regions: high altitude (above ~50 km) and low altitude (below ~50 km). The interferers included in the high altitude portion of version 4 P/T analysis are presented in Table A3, and the interferers for the low altitude portion of the analysis are given in Table A4. VMR profiles for interferers are retrieved simultaneously with pressure and temperature during the analysis, using different profiles for different isotopologues of the same molecule.

For the high altitude portion of the analysis, where aerosols and atmospheric refraction do not impact instrument pointing, separations between measurement tangent heights can be accurately calculated from the STK software using knowledge of the satellite orbit. In the high altitude region, an empirical function is employed to retrieve a VMR profile for main isotopologue CO₂ [6]. For the altitude region above the highest analyzed measurement (~125 km), no information is available from which to determine the shape of the VMR profile. Therefore, an assumed VMR profile shape is chosen, and a constant scaling factor as a function of altitude (determined during the least-squares analysis) is used to account for the contribution to the calculated spectrum from the altitude region above the highest analyzed measurement.

As mentioned previously, however, some occultations exhibit enhancements in CO₂ absorption at high altitudes, likely a consequence of non-LTE effects. Using the typical shape assumed for the CO₂ VMR profile (decreasing with increasing altitude) can lead to an underestimate of the contribution from the altitude region above the highest analyzed measurement, resulting in an upward “hook” in the VMR profile near the upper altitude limit of the retrieval.

To minimize this problem, version 4 processing features a pre-retrieval to determine an effective shape for the CO₂ VMR profile above 110 km, carried out prior to the full P/T analysis. The microwindow set employed in this pre-retrieval, consisting of some

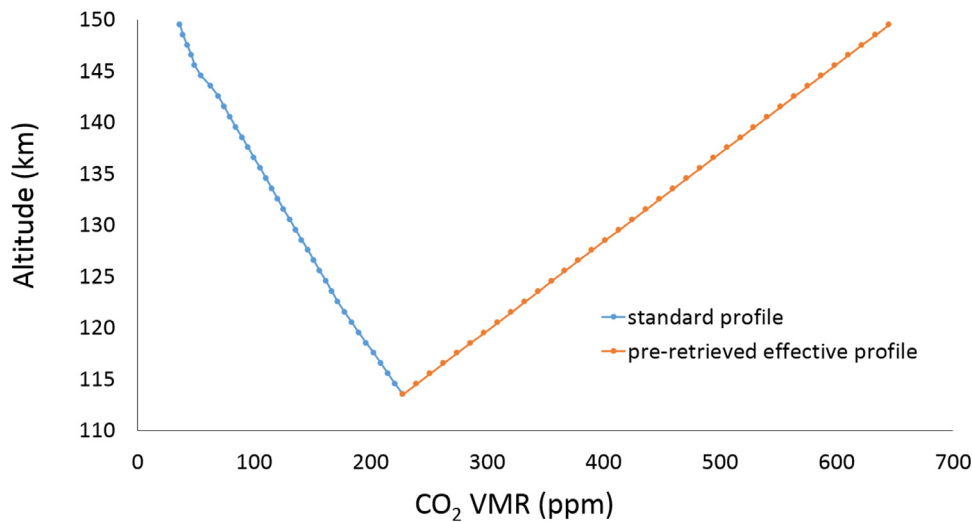


Fig. 8. The pre-retrieved effective CO₂ VMR profile (in orange) from measurements between 110 and 140 km for occultation ss70730, an occultation that exhibits enhanced CO₂ absorption at high altitude. The standard CO₂ VMR profile shape (in blue) employed in previous processing versions is shown for comparison. (For interpretation of the references to color in this figure legend, the reader is referred to the web version of this article.)

of the strongest lines in the CO₂ ν_3 band, is presented in Table A5. Pressure and temperature profiles are fixed to the calculations from the NRLMSISE-00 software, while tangent heights for analyzed measurements are values calculated from the STK software. These quantities may not have high accuracy but are sufficient to generate an estimate for the effective shape of the CO₂ VMR profile required in this altitude region. A linear variation with altitude is assumed for the CO₂ VMR profile, requiring two parameters (the VMR value in the tangent layer of the lowest analyzed measurement plus the vertical slope) that are determined via least squares fitting. Fig. 8 shows results for the occultation mentioned previously (ss70730) that had CO₂ spectral features in measurements above 160 km. The blue curve is the standard profile shape for CO₂ employed in this altitude region for previous processing versions, and the orange curve is the effective shape resulting from the version 4 pre-retrieval. The orange curve exhibits strong growth with increasing altitude rather than the decrease assumed previously, providing a much improved characterization of the contribution from the altitude region above ~125 km for subsequent processing.

Keep in mind that this is not an attempt to characterize CO₂ itself above 125 km. It is a means to reduce the contribution from problems in the altitude region above 125 km to errors in the altitude region below 125 km, mimicking the enhanced absorption from increasing non-LTE as a function of altitude using an effective shape for the CO₂ VMR profile that increases with altitude.

Between ~45 and 18 km, tangent height separations are calculated from hydrostatic equilibrium, as was done for version 3 retrievals [7]. This is accomplished through fitting CO₂ lines (using the microwindows described in Table A2) while fixing CO₂ VMR to an assumed profile. In processing versions prior to version 4, the assumed variation of CO₂ VMR with time [6] was too low compared to independent measurements of CO₂ reported over the span of the ACE mission. Because the assumed CO₂ VMR profile is used to derive a pressure profile from ACE-FTS measurements, this low bias was reflected in the trends for all retrieved molecules. For version 4, a new model is used to generate a priori CO₂ VMR profiles [33] that features an improved time variation and also includes variations with location and season, which were missing from the CO₂ VMR profiles generated for previous processing versions. Fig. 9 shows the growing difference of assumed mid-stratospheric CO₂ in version 4 relative to previous processing versions. In early 2020,

this amounts to a ~2.5% difference, which would translate to a ~0.16%/year difference in derived trends from the new data set.

The lowest analyzed measurement in the low altitude P/T analysis (which spans the altitude range ~18 to ~50 km) is the highest analyzed measurement used in the N₂ continuum analysis. The tangent height determined for this measurement from the N₂ continuum is used to generate an absolute altitude registration for the results above 18 km (which are analyzed in terms of tangent height separations). The tangent pressure determined for the measurement from the N₂ continuum analysis is fixed during the low altitude P/T analysis in order to ensure no discontinuities in the retrieved pressure profile. The tangent temperature for this measurement, however, is not fixed during the low altitude P/T analysis. It is retrieved. Many of the CO₂ lines employed in P/T analysis near 18 km (from the microwindow set in Table A2) are highly sensitive to temperature. If temperatures from the model are in error by even a small amount (e.g., 0.5–1 K), fixing the tangent temperature can lead to instability in the least squares fitting.

When tangent heights for analyzed measurements are too close together, retrievals can get unstable, in some cases generating large fluctuations in retrieved profiles. In these situations, the least squares fitting has the flexibility to gain a small (typically a fraction of a percent) improvement in the goodness of fit parameter (χ^2) by inducing a “burst” of superimposed oscillatory behavior on the retrieved profile. ACE-FTS measurement encompass a relatively large range of tangent height separations, from ~1.5 km at high altitude for some occultations up to ~6 km at high altitude for others, depending on the angle between the orbital plane and the look direction to the Sun (called the “beta angle”) for the given occultation. Tangent height separations also decrease with decreasing altitude below ~40 km as increasing refraction effects cause the measurements to crowd closer and closer together. For occultations with small tangent height separations (high beta angle), constraints in pressure/temperature retrievals are sometimes needed at lower altitude (near 18 km, the lower altitude limit in these retrievals, where you can get measurements that are a few hundred meters apart for an occultation with a very large beta angle) in order to avoid instabilities.

Prior to version 4, analysis was limited to no more than one measurement in each layer of the 1 km grid. “Excess” measure-

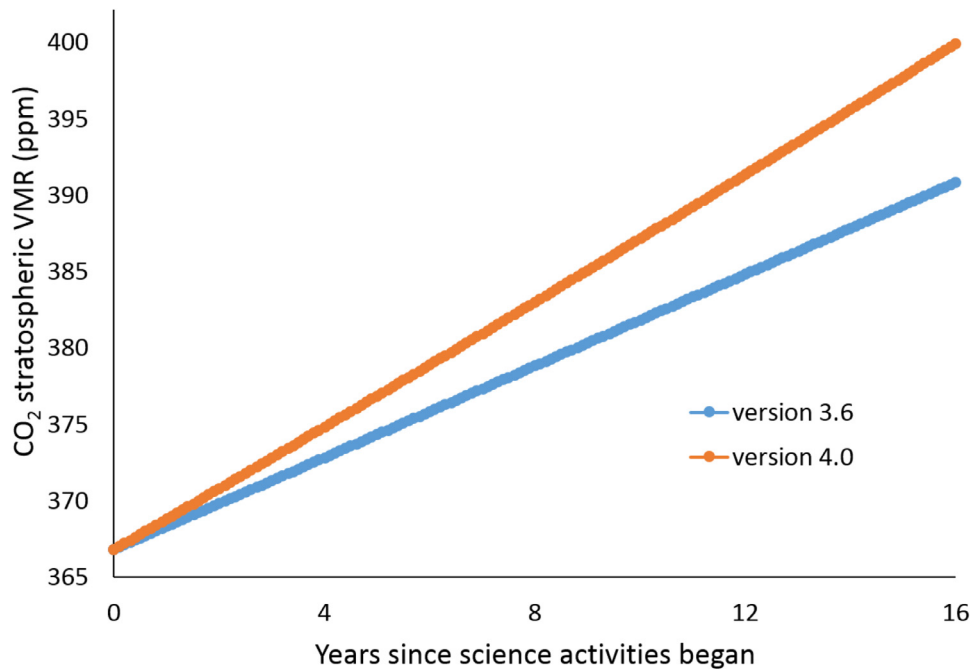


Fig. 9. Divergence in assumed mid-stratospheric CO₂ between versions 3.6 (in blue) and 4.0 (in orange) since the beginning of scientific measurements for the ACE-FTS mission. (For interpretation of the references to color in this figure legend, the reader is referred to the web version of this article.)

ments from a given layer were simply excluded from analysis. This is done in the P/T retrieval because accurate pointing information for the ACE-FTS instrument is not available, and measurement tangent heights therefore need to be determined through analysis of ACE-FTS spectra. Two quantities are being derived for each measurement: tangent pressure and tangent temperature, with tangent height separations between measurements calculated based on these quantities. A set of spectral lines provides two pieces of information: the relative intensities of different lines gives a measure of the temperature, while the absolute intensities allows you to derive pressure. Analyzing every measurement with the chosen method would require decoupling the determination of tangent height separations from the determination of tangent pressures and temperatures, which would leave the analysis under-constrained.

Note that tangent heights for the skipped measurements are determined at the end of the pressure/temperature retrieval, and these measurements are employed in the subsequent VMR retrievals. No measurements are ever excluded from the VMR retrievals unless they are excessively noisy.

Version 4 employs a constraint on the separation between analyzed measurements for the low altitude P/T analysis: a minimum of 2 km for tangent heights above 19.5 km, and a minimum of 1.5 km below that. Using a coarser altitude grid (compared to previous processing versions) suppresses unphysical oscillations in retrieved pressure and temperature profiles, promoting smoother results. Note that at low altitudes, pressure broadening makes the lines broader than the instrumental line shape, which provides additional information (line widths) in the analysis, making retrieved profiles less prone to unphysical oscillations, and so a smaller tangent height separation can be used.

Some of the microwindows in Table A2 contain N₂ quadrupole lines rather than CO₂. P/T analysis requires an assumption for the VMR profile of CO₂, but the VMR profile of N₂ is well known at low altitudes (in dry air, a constant 0.7809 as a function of altitude). Therefore, including N₂ lines in the analysis provides additional information without requiring extra assumptions or additional fitting parameters. Unfortunately, the number and the strength of N₂

quadrupole lines are insufficient to perform the P/T analysis on the basis of those lines alone from ACE-FTS measurements.

4.3. Volume mixing ratio retrievals

After the pressure and temperature profiles, along with tangent heights for all of the measurements, are determined for a given occultation, VMR profiles for various atmospheric constituents are derived.

Prior to version 4, a global least squares fitting approach determined the VMR of the target constituent at each measurement tangent height contained within the altitude range of the microwindow set. When multiple measurements occurred within a particular layer on the 1 km altitude grid, a single VMR value was determined corresponding to the center of the layer rather than having multiple values corresponding to the individual tangent heights, although every measurement was still fitted. VMR values on the 1 km grid, required for forward model calculations, were populated through piecewise quadratic interpolation from the quantities on the retrieval grid (also referred to as the “tangent grid”).

As discussed for P/T analysis, when the altitude spacing on the retrieval grid is too small, retrievals risk inducing unphysical oscillations in the derived profiles. For version 4, a minimum spacing is imposed on the retrieval grid to suppress unphysical oscillations. Above 15 km, the minimum altitude spacing in the retrieval grid is 2 km, while below 15 km, the minimum spacing is 1 km. If the measurement spacing in the occultation is larger than the minimum spacing at all altitudes, then the retrieval grid points will correspond to the measurement tangent heights, as before. If the altitude difference between tangent heights drops below the minimum spacing, then retrieval grid points partially decouple from the measurement tangent heights. Starting from the highest analyzed measurement and moving downward in altitude, retrieval grid points are chosen either at the tangent height of the first measurement below the previous retrieval grid point (if the spacing is greater than or equal to the minimum) or in the center of a layer on the 1 km grid such that the altitude difference from the previous grid point is greater than or equal to the mini-

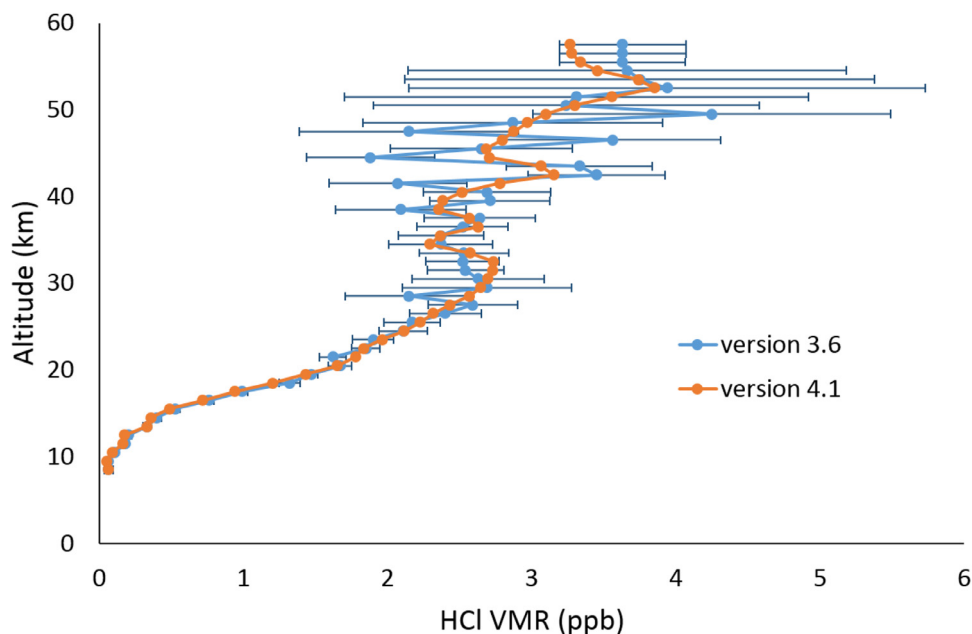


Fig. 10. The retrieved HCl VMR profile from sr52149 from version 3.6 (in blue) and version 4.1 (in orange), plotted on the standard 1 km grid (not the retrieval grid). The version 3.6 result exhibits unphysical oscillations in the retrieved profile. Error bars for version 3.6 are the random fitting errors from the least squares analysis. Errors for version 4.1 (not shown) are generally smaller than those from version 3.6. (For interpretation of the references to color in this figure legend, the reader is referred to the web version of this article.)

imum spacing. This approach limits altitude spacing on the retrieval grid while ensuring sufficient information for the least squares fitting: e.g., one could not retrieve VMRs on a 2 km altitude grid if the measurements were 4 km apart without imposing additional constraints. Again, although a coarser altitude grid is employed in the retrieval, all measurements within the altitude range of the microwindows are analysed.

Fig. 10 shows the effect of introducing the constraint on the retrieval grid for version 4.1 in occultation sr52149. With a relatively small altitude spacing between measurements (roughly 1.6 km near 50 km), when fitting on an altitude grid that follows the tangent height, the analysis gains a tiny improvement in fitting residuals by inducing a burst of oscillatory behavior, as seen in the version 3.6 profile in Fig. 10. The larger altitude separations between fitted quantities in version 4.1 suppress these oscillations. The two results agree within their errors (as evident from the error bars in Fig. 10, shown only for version 3.6), but the oscillation in version 3.6 is a numerical artifact that does not reflect true altitude structure in the VMR profile.

Heavier atmospheric molecules (e.g., CFCs, acetone, PAN, etc.) have broad spectral features in the infrared, unlike lighter molecules that tend to have sharp lines. In ACE-FTS spectra, H₂O lines typically have large systematic residuals in the troposphere, as mentioned previously, and line mixing effects in CH₄ often give rise to enhanced residuals that extend into the stratosphere [27]. When lines from one or both of these molecules overlap the absorption feature from a heavy molecule, elevated residuals from the lines can degrade the quality of the retrieval for the heavy molecule, particularly when the absorption feature for the heavy molecule is weak. To minimize problems from H₂O and CH₄ (and other sources of enhanced residuals), version 4 employs a set of “microwindow slices” across the broad absorption feature(s) of a heavy molecule rather than a single, wide window (as was done with previous processing versions). A common set of baseline parameters (baseline scaling and baseline slope, used to account for things like aerosol contributions missing from the calcu-

lated spectrum) is used for the set of microwindow slices, rather than fitting for separate baseline parameters in the individual windows.

Fig. 11 shows the residuals obtained from fitting N₂O₅ in occultation sr11613. The residuals in Fig. 11a result from using a single broad window and Voigt line shapes for interfering lines, with spectroscopic parameters taken from HITRAN 2016. Large features in the residuals from an H₂O line (only for measurements below 18 km, the tropopause for this measurement) and two CH₄ lines with relatively strong line mixing (with enhanced residuals that extend into the stratosphere) are indicated in the plot. Additional CH₄ lines in the microwindow exhibit less pronounced (but still significant) systematic residuals from line mixing in this wavenumber region. In version 4.0 (not shown in Fig. 11), selected CH₄ lines in the region employed line mixing and had line strengths adjusted to improve fitting residuals for N₂O₅, thereby reducing systematic errors for the molecule. In version 4.1, it was found that further improvements to the residuals could be achieved by adjusting more parameters and using more complicated line shapes for some lines, while leaving line strengths unchanged from the values provided in HITRAN 2016.

Fig. 11b shows the residuals obtained with adjustments made to the line list for version 4.1. Similar to the non-Voigt adjustments made in the N₂ continuum region (Section 4.2.1), qSDV was used for N₂O lines in the region, while CH₄ lines with significant residuals in Fig. 11a used Voigt with line mixing, qSDV, or qSDVLM line shapes, depending on which gave the best residuals. For these lines, pressure broadening parameters and pressure shifts were adjusted along with the determination of non-Voigt parameters from the analysis of ACE-FTS spectra, while all other parameters (line positions, line strengths, lower state energies, temperature exponent, etc.) were fixed to their values from HITRAN 2016. Assumed temperature dependences were the same as described in Section 4.2.1. The non-Voigt spectroscopic parameters for CH₄ and N₂O, employed in version 4.1 analysis in the vicinity of the N₂O₅ spectral feature, are included in the supplemental file

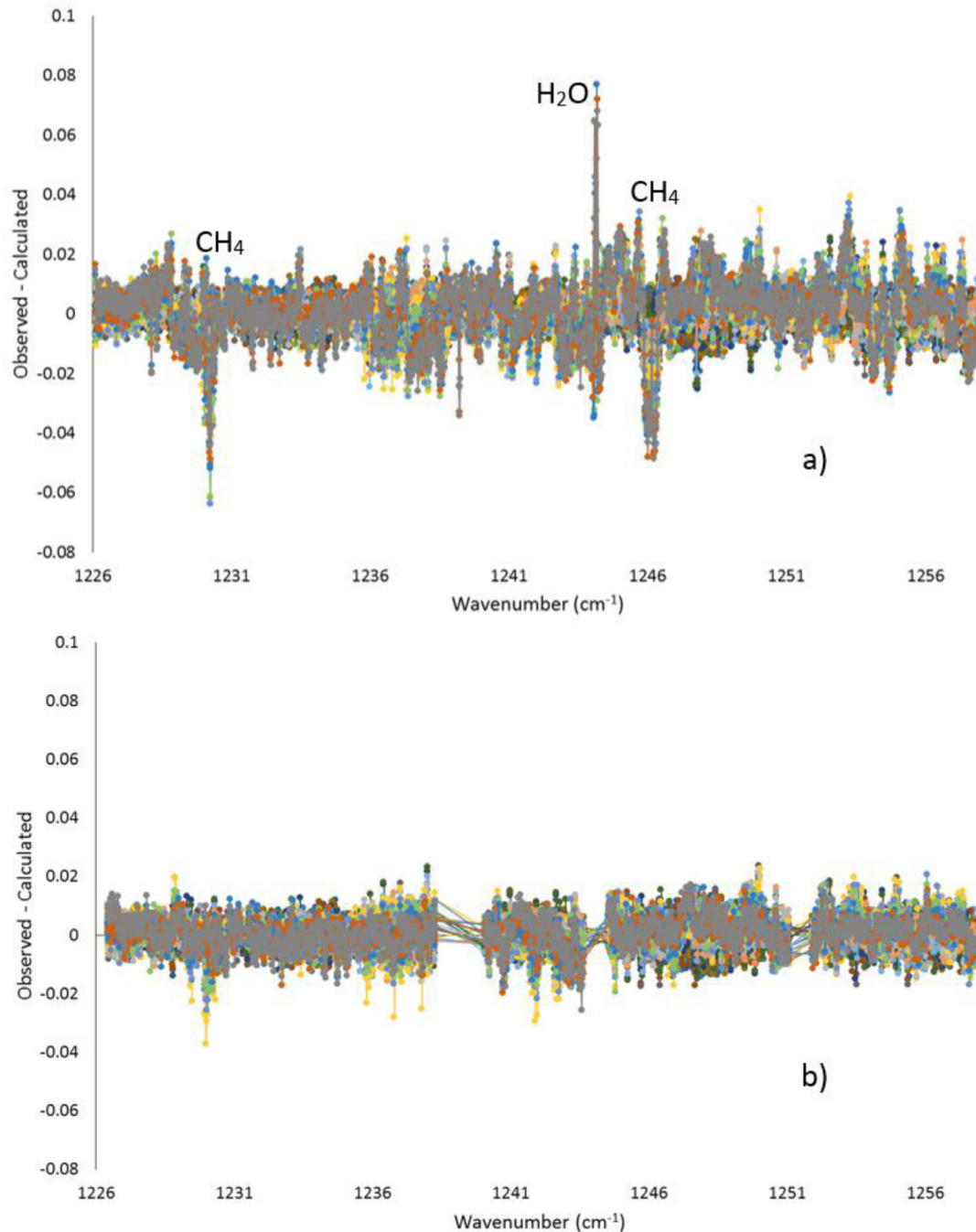


Fig. 11. Residuals for all measurements between 12 and 45 km (a total of 21 measurements) in occultation ss11613 in the vicinity of the N_2O_5 spectral feature. a) Residuals using Voigt line shapes for all lines, with spectroscopic parameters from HITRAN 2016. b) Residuals using the line list employed in version 4.1 processing, with non-Voigt line shapes applied to N_2O and CH_4 lines in the wavenumber region.

(ACEFTS_v4.1_nonVoigt.txt). Again, these parameters may not work well for pressure and temperature conditions outside the relatively narrow range from which they were derived.

As mentioned previously, the version 4 microwindow set for N_2O_5 employs the “microwindow slice” approach: a collection of microwindows that all use a common set of baseline parameters (baseline scale and baseline slope), rather than having separate baseline parameters in each window, which would serve to obscure information on the broad N_2O_5 spectral feature. The gaps in the residuals in Fig. 11b are a consequence of this, from wavenumber regions containing H_2O lines having been excised from the re-

trieval. There remain features greater than the noise in Fig. 11b, but there is a dramatic improvement in the residuals compared to version 3.6.

5. ACE-Imagers

Analysis of measurements from the imagers onboard SCISAT employ the set of imager pixels coincident with the center of the ACE-FTS field of view. For each measured image, an average transmittance is calculated from this set of pixels [5], and the corresponding tangent height is interpolated from tangent heights de-

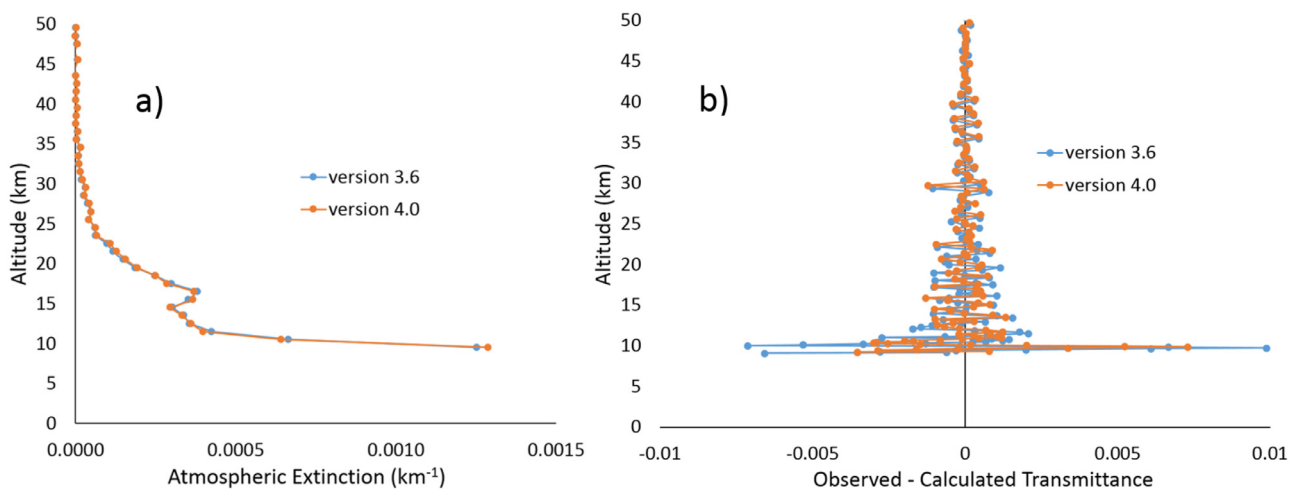


Fig. 12. a) Retrieved atmospheric extinction profiles from version 3.6 (in blue) and version 4.0 (in orange) for the near infrared imager (at wavelength $1.02 \mu\text{m}$) for occultation ss73988. b) Residuals for the fitted transmittances as a function of tangent altitude. (For interpretation of the references to color in this figure legend, the reader is referred to the web version of this article.)

terminated for ACE-FTS measurements. Atmospheric extinction profiles are generated by inverting the transmittances through a global least squares analysis. In all processing versions, a 1 km altitude grid is employed as the retrieval grid. For previous processing versions, forward model calculations were conducted on the same 1 km altitude grid. For version 4, forward model calculations occur on a 100 m altitude grid.

Fig. 12 shows the retrieved atmospheric extinction profiles from the near infrared imager for occultation ss73988, along with the fitting residuals (plotted as a function of the tangent heights for the transmittance data). From the residuals, it is evident that the 100 m calculation grid in version 4 processing yields improved agreement between measurement and calculation where extinction varies rapidly with altitude, suggesting the version 4.0 profile (and version 4.1, which has similar results for this occultation) provides an improved representation of the atmosphere compared to version 3.6 results.

In previous processing versions, extinction values were determined in each layer on the 1 km altitude grid, even when no transmittance tangent heights were within a given layer (in instances where imager data were lost during downlink from the satellite to the ground station), which typically led to spikes in the retrieved profile for occultations with altitude gaps in the measurements. In version 4, extinction values are only retrieved in layers on the 1 km grid containing at least one measurement tangent height, suppressing unphysical spikes but leading to altitude gaps in the reported imager profiles for such occultations.

6. Version 4 data products

The ACE-FTS version 4 dataset includes atmospheric temperature, pressure, and atmospheric constituents that were in the previous processing version: O_3 , H_2O , N_2O , CO , CH_4 , NO , NO_2 , HNO_3 , HF , HCl , OCS , N_2O_5 , ClONO_2 , HCN , CH_3Cl , CF_4 , CCl_4 , CFC-11 , CFC-12 , CFC-113 , HCFC-22 , HCFC-141b , HCFC-142b , COCl_2 , COF_2 , COClF , C_2H_6 , C_2H_2 , HCOOH , SF_6 , HO_2NO_2 , H_2O_2 , H_2CO , CH_3OH , N_2 , O_2 , and CO_2 above ~ 60 km, along with subsidiary isotopologues H_2^{18}O , H_2^{17}O , HDO , $^{13}\text{CO}_2$, ^{18}OCO , ^{17}OCO , $^{18}\text{O}^{13}\text{CO}$, ^{18}OOO , O^{18}OO , O^{17}OO , ^{15}NNO , N^{15}NO , N_2^{18}O , N_2^{17}O , ^{13}CO , C^{18}O , C^{17}O , $^{13}\text{CH}_4$, CH_3D , OC^{34}S , and O^{13}CS .

Additionally, version 4 includes the following constituents: ClO , SO_2 , CH_3CN , HFC-134a , HFC-23 , $\text{C}_3\text{H}_6\text{O}$ (acetone), $\text{C}_2\text{H}_3\text{NO}_5$ (PAN), and CO_2 below 18 km [22], along with isotopologues ^{17}OOO , H^{15}NO_3 , and $^{15}\text{NO}_2$. Some of these molecules were studied previously using “research products” (e.g., [34]) generated from ACE-FTS measurements during development of the version 4 processing software.

ACE data are freely available upon registration. Request for access to the data can be made at <https://database.scisat.ca/2signup.php>. A document describing the microwindow sets for all version 4 data products is available on the data distribution web site.

Fig. 13 shows seasonal latitude distribution plots for version 4.0 ClO , one of the new molecules included in this processing version. Periods of strong enhancement during polar winter/spring chlorine processing events are evident in the plots, with significantly stronger enhancement in the Antarctic than is observed in the Arctic, as expected [35]. Absorption features for this molecule are very weak outside the periods of strong enhancement, and there was some concern as to the quality of results that could be achieved under “background” conditions. In Fig. 13, blank (white) regions indicate where the average VMR was negative, an unphysical result. This could be a sign of problems with the retrievals for the conditions in those regions, but it might also be a symptom of diurnal effects, i.e., variations in ClO VMR along the line of sight (resulting from different lengths of time spent in sunlight for different atmospheric regions) that are significantly different from the symmetric atmosphere implicitly assumed in forward model calculations.

Structure in the results for different seasons (e.g., Fig. 13b for June–July–August versus Fig. 13d for December–January–February) show promise that ACE-FTS version 4 ClO data might be viable for scientific analysis under background conditions, with sufficient averaging. ClO levels are very low in polar regions experiencing long daylight hours (e.g., the Arctic during Northern Hemisphere summer).

Similarly, atmospheric SO_2 exhibits periodic strong enhancements in volcanic plumes but is currently at low levels under background conditions. There was some question of the quality expected for ACE-FTS version 4 SO_2 results under background conditions, but a recent study using a research product for SO_2 gen-

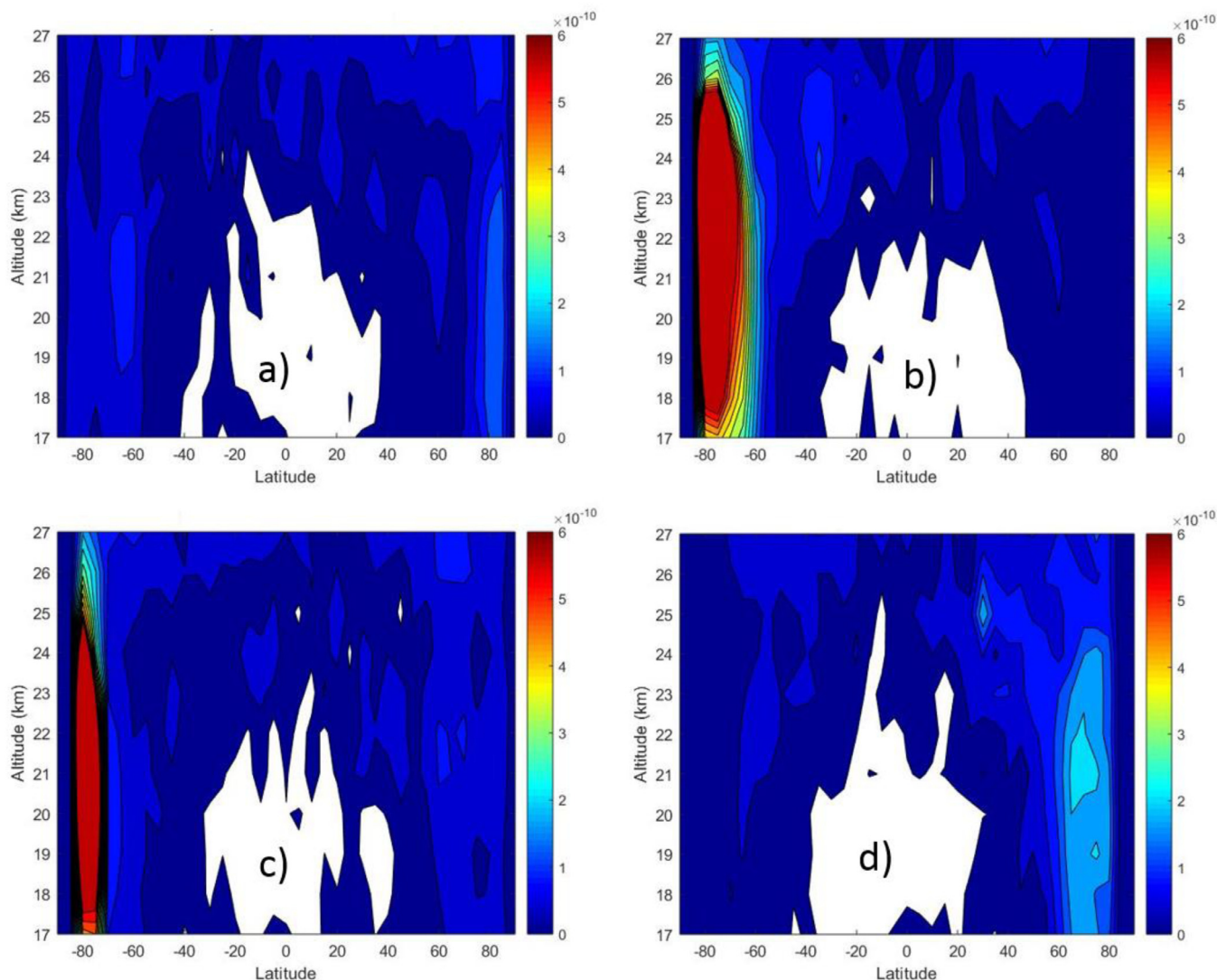


Fig. 13. ACE-FTS version 4.0 ClO averaged from 2004 to 2019 for a) Northern Hemisphere spring (March–April–May), b) Northern Hemisphere summer (June–July–August), c) Northern Hemisphere autumn (September–October–November), and d) Northern Hemisphere winter (December–January–February). ClO VMR values are indicated by the color scale to the right of the plots.

erated from ACE-FTS measurements [36] indicates that the instrument provides reasonable results under such conditions.

7. Conclusion

Version 4 processing for the ACE-FTS instrument and the imagers onboard the SCISAT satellite has been implemented. It makes use of the latest available spectroscopic information, updates the microwindow sets for a number of molecules compared to the previous processing version, and provides ten atmospheric constituents that were not included in version 3 (acetone, PAN, HFC-23, CH_3CN , HFC-134a, ClO, SO_2 , $^{15}\text{NO}_2$, ^{17}OOO , H^{15}NO_3 , and $^{15}\text{NO}_2$), as well as CO_2 below 18 km. Efforts were made to improve the accuracy of forward model calculations, improve software robustness, and minimize incidences of unphysical oscillations in retrieved profiles.

Version 4.1, the most recent processing version, addresses problems encountered in version 4.0 for occultations containing strong aerosol signatures (e.g., from polar stratospheric clouds) in the vicinity of the N_2 continuum (near 2500 cm^{-1}).

Requests to access version 4 data through the distribution web site can be made at <https://database.scisat.ca/2signup.php>.

Declaration of Competing Interest

The authors declare that they have no known competing financial interests or personal relationships that could have appeared to influence the work reported in this paper.

CRediT authorship contribution statement

C.D. Boone: Conceptualization, Software, Visualization, Writing - original draft. **P.F. Bernath:** Supervision, Writing - review & editing. **D. Cok:** Project administration, Visualization. **S.C. Jones:** Software. **J. Steffen:** Resources.

Acknowledgments

Funding was provided by the [Canadian Space Agency](#) (grant number 9F045-180032/001/MTB SCISAT). Thanks to Yves Rochon for providing the updated pressure and temperature data from the Canadian Meteorological centre.

Appendix A

Table A1
Microwindow set for version 4.1 N₂ continuum analysis.

Center (cm ⁻¹)	Width (cm ⁻¹)	Not Fit (cm ⁻¹)	Center (cm ⁻¹)	Width (cm ⁻¹)	Not Fit (cm ⁻¹)
1959.55 ^a	0.50		2507.75	1.18	
1980.01 ^b	0.30		2510.05	1.30	
2420.80	1.20		2511.00	0.60	
2421.70	1.20		2513.40	0.60	
2424.50	1.00		2516.90	0.80	
2425.45	0.90		2519.15	0.50	
2427.00	1.00		2521.67	0.50	
2429.40	0.40		2524.00	0.60	
2430.25	0.50	0.20	2528.21	0.30	
2431.84	1.00	0.70	2538.85	0.50	
2434.70	0.40		2539.85	0.50	
2439.68	0.72	0.54	2545.87	0.26	
2441.00	0.40		2552.40	0.40	
2444.51	0.30		2560.39	0.30	
2449.20	1.00	0.70	2563.12	0.24	
2454.40	1.20	0.80	2572.10	0.80	0.64
2461.25	0.50	0.22	2594.02	0.60	0.50
2469.61	0.90	0.50	2603.22	0.60	0.42
2478.82	0.40		2610.95	1.10	
2481.00	0.80	0.40	2615.65	0.70	
2488.96	0.44		2617.28	0.56	0.38
2489.76	0.40		2620.75	0.50	
2491.26	0.40		2633.90	0.40	0.25
2492.00	0.40		2636.31	0.30	0.18
2492.74	0.40		2650.43	0.34	
2496.77	0.86		2653.75	0.50	
2497.80	0.80		2661.45	0.50	
2498.67	0.94		2663.30 ^c	0.60	
2499.70	0.40		2668.21	0.30	
2501.05	0.70		2673.55	0.70	0.44
2502.02	1.24		2679.20	0.40	
2503.11	0.38		2687.53	1.10	0.90
2503.80	0.60		2700.30	0.80	
2505.25	0.50		2713.75 ^d	0.70	
2506.10	0.80		2732.52 ^e	0.64	
2506.67	0.34		3160.15 ^b	0.50	

"Not Fit": portion of the microwindow assigned zero weighting in least squares fitting (see text).

^a Outside window for H₂O, tangent height > 10 km.

^b Outside window for CO₂.

^c Outside window for HDO, tangent height > 14 - 7 * sin²(latitude).

^d Outside window for HDO, tangent height < 14 - 7 * sin²(latitude).

^e Outside window for H₂O, tangent height < 10 km.

Table A2
Microwindow set for version 4.1 pressure/temperature analysis.

Center (cm ⁻¹)	Width (cm ⁻¹)	Lower limit (km)	Upper limit (km)	Center (cm ⁻¹)	Width (cm ⁻¹)	Lower limit (km)	Upper limit (km)
1898.85	0.3	15	30	2320.51 ³	0.3	82	95
1899.17	0.3	35	58	2321.13	0.3	108	125
1902.17	0.3	40	60	2332.37	0.3	111	125
1906.47	0.3	45	65	2339.45	0.3	112	125
1910.95	0.3	47	68	2344.41	0.3	110	125
1912.51	0.3	48	68	2345.95	0.3	110	125
1914.03	0.3	48	70	2349.91	0.3	105	117
1917.07	0.3	48	70	2351.45	0.3	109	122
1920.11	0.3	47	70	2354.49	0.3	110	125
1924.71	0.3	41	65	2355.79	0.3	111	125
1929.35	0.3	32	50	2358.73	0.3	112	125
1934.01	0.5	32	60	2361.45	0.3	110	125
1941.17	0.3	15	45	2364.11	0.3	110	125
1944.36	0.24	15	30	2366.63	0.3	110	125
1950.69	0.26	15	45	2367.89	0.3	110	125
1962.76 ^a	0.24	15	40	2369.17	0.3	110	125
1966.85	0.3	15	45	2370.27	0.3	109	125

(continued on next page)

Table A2 (continued)

Center (cm ⁻¹)	Width (cm ⁻¹)	Lower limit (km)	Upper limit (km)	Center (cm ⁻¹)	Width (cm ⁻¹)	Lower limit (km)	Upper limit (km)
1970.31	0.3	15	45	2371.43	0.3	108	125
1971.77	0.3	15	45	2372.55	0.3	107	125
1975.11	0.3	15	40	2373.67	0.3	105	125
1980.01	0.3	15	25	2374.75	0.3	103	125
1981.7	0.4	15	25	2375.81	0.3	101	125
2035.29	0.3	50	60	2376.85	0.3	99	125
2038.41	0.3	47	62	2377.85	0.3	97	125
2040.03	0.3	42	65	2378.83	0.3	94	125
2042.95	0.3	48	68	2379.79	0.3	90	120
2044.51	0.3	50	70	2380.71	0.3	86	115
2045.97	0.3	52	72	2381.61	0.3	83	111
2047.53	0.3	53	73	2382.47	0.3	82	106
2049.05	0.3	55	75	2383.35	0.3	81	101
2052.11	0.3	58	79	2384.21	0.3	79	95
2053.65	0.3	59	80	2385.01	0.3	77	90
2056.71	0.3	63	85	2385.79	0.3	71	85
2058.25	0.3	63	85	2386.51	0.3	69	83
2061.33	0.3	64	85	2387.25	0.3	66	80
2062.87	0.3	63	85	2387.95	0.3	64	78
2066.03	0.3	63	84	2388.34 ^d	0.2	25	45
2067.53	0.3	62	83	2388.65	0.3	61	75
2070.63	0.3	61	80	2389.29	0.3	58	71
2072.23	0.3	62	80	2389.93	0.3	55	68
2249.69 ^b	0.3	80	95	2390.51	0.3	52	65
2277.35	0.3	60	75	2391.13	0.3	49	64
2282.26	0.24	64	78	2391.71	0.3	45	60
2284.51	0.3	65	80	2392.21	0.3	40	55
2289.35	0.3	72	85	2392.61	0.3	17	50
2291.45	0.3	77	92	2393.05	0.3	17	50
2293.81	0.3	79	99	2393.8	0.6	25	50
2296.05	0.3	80	101	2393.97	0.3	17	25
2298.25	0.3	82	115	2395.99 ^d	0.22	25	40
2299.21 ^c	0.3	75	90	2403	0.24	17	40
2300.37	0.3	84	120	2403.55 ^d	0.3	20	45
2304.85	0.3	91	122	2408.85	0.3	17	48
2306.97	0.3	94	123	2411.17 ^d	0.22	15	40
2309.05	0.3	97	125	2418.65 ^d	0.3	35	45
2311.11	0.3	99	125	2421.26	0.24	17	48
2313.11	0.3	101	125	2433.62 ^d	0.24	30	45
2319.15	0.3	107	125				

^a Microwindow contains O₃ spectra features.

^b Microwindow contains a ¹³CO₂ (CO₂ isotopologue 2) line.

^c Microwindow contains an ¹⁸OCO (CO₂ isotopologue 3) line.

^d Microwindow contains an N₂ quadrupole line.

Table A3

Interferers in the high-altitude portion (> ~50 km) of the P/T analysis.

Interferer	Lower altitude (km)	Upper altitude (km)
¹⁸ OCO	69	100
¹⁷ OCO	69	100

Table A4

Interferers in the low-altitude portion (< ~50 km) of the P/T analysis.

Interferer	Lower altitude (km)	Upper altitude (km)
O ₃	18	50
COF ₂	18	30

Table A5

Microwindow set for pre-retrieval of the effective shape of the CO₂ VMR profile in the altitude region above the highest analyzed measurement (~125 km).

Center (cm ⁻¹)	Width (cm ⁻¹)	Lower limit (km)	Upper limit (km)
2361.45	0.30	110	140
2364.1	0.30	110	140
2366.63	0.30	110	140
2367.88	0.30	110	140
2369.1	0.30	110	140
2370.27	0.35	110	140
2371.43	0.30	110	140
2372.56	0.30	110	140
2373.67	0.35	110	140
2374.75	0.40	110	140

References

- [1] Bernath PF, McElroy CT, Abrams MC, Boone CD, Butler M, Camy-Peyret C, et al. Atmospheric Chemistry Experiment (ACE): mission overview. *Geophys Res Lett* 2005;32:L15S01. doi:10.1029/2005GL022386.
- [2] Bernath PF. The atmospheric chemistry experiment (ACE). *J Quant Spectrosc Radiat Transf* 2017;186:3–16.
- [3] Bujis HL, Soucy M-A, Lachance RL. ACE-FTS hardware and level 1 processing. In: Bernath Peter F, editor. *The atmospheric chemistry experiment ACE at 10: a solar occultation anthology*. Virginia: A. Deepak Publishing; 2013. p. 53–80.
- [4] McElroy CT, Nowlan CR, Drummond JR, Bernath PF, Barton DV, Dufour DG, et al. The ACE-Maestro instrument on SCISAT: description, performance, and preliminary results. *Appl Opt* 2007;46:4341–56.
- [5] Gilbert KL, Turnbull DN, Walker KA, Boone CD, McLeod SD, Butler M, et al. The onboard imagers for the Canadian ACE SCISAT-1 mission. *J Geophys Res* 2007;112:D12207.
- [6] Boone CD, Nassar R, Walker KA, Rochon Y, McLeod SD, Rinsland CP, Bernath PF. Retrievals for the atmospheric chemistry experiment Fourier-transform spectrometer. *Appl Opt* 2005;44(33):7218–31.
- [7] Boone CD, Walker KA, Bernath PF. Version 3 retrievals for the atmospheric chemistry experiment Fourier transform spectrometer (ACE-FTS). In:

- Bernath Peter F, editor. The atmospheric chemistry experiment ace at 10: a solar occultation anthology. Virginia: A Deepak Publishing; 2013. p. 103–27.
- [8] Buehner M, McTaggart-Cowan R, Beaulne A, Charette C, Garand L, Heilliette S, et al. Implementation of deterministic weather forecasting systems based on ensemble-variational data assimilation at environment Canada. Part I: the global system. *Mon Weather Rev* 2015;143:2532–59.
- [9] Picone JM, Hedin AE, Drob DP, Aikin AC. NRLMSIS-00 empirical model of the atmosphere: statistical comparisons and scientific issues. *J Geophys Res* 2002;107(A12):1468–83.
- [10] <ftp://ftp.agi.com/pub/DynamicEarthData/stkFluxReadme.txt>.
- [11] Mertens CJ, Mlynczak MG, López-Puertas M, Wintersteiner PP, Picard RH, et al. Retrieval of mesospheric and lower thermospheric kinetic temperature from measurements of CO₂ 15 μm Earth limb emission under non-LTE conditions. *Geophys Res Lett* 2001;28:1391–4.
- [12] Chaparro L. Signals and systems using MATLAB. second ed. Academic Press; 2015.
- [13] Carlotti M. Global-fit approach to the analysis of limb scanning atmospheric measurements. *Appl Opt* 1988;27:3250–4.
- [14] Press WH, Flannery BP, Teukolsky SA, Vetterling WT. Numerical recipes in Fortran. second ed. Cambridge University; 1992.
- [15] Gordon IE, Rothman LS, Hill C, Kochanov RV, Tan Y, Bernath PF, et al. The HITRAN 2016 molecular spectroscopic database. *J Quant Spectrosc Radiat Transf* 2017;203:3–69.
- [16] Perrin A, Toon G, Orphal J. Detection of atmospheric 15NO₂ in the ν₃ spectral region (6.3 μm). *J Quant Spectrosc Radiat Transf* 2015;154:91–7.
- [17] Perrin A, Demaison J, Toon G. The ν₁, ν₂, and ν₃ bands of carbonyl chlorofluoride (COFCI) at 5.3, 9.1, and 13.1 μm: position and intensity parameters and their use for atmospheric studies. *J Quant Spectrosc Radiat Transf* 2011;112:1266–79.
- [18] Boone CD, Bernath PF. The instrumental line shape of the atmospheric chemistry experiment Fourier transform spectrometer (ACE-FTS). *J Quant Spectrosc Radiat Transf* 2019;230:1–12.
- [19] Rodgers CD. Inverse methods for atmospheric sounding, theory and practice. Singapore: World Scientific; 2000.
- [20] Dudhia A. The reference forward model (RFM). *J Quant Spectrosc Radiat Transf* 2017;186:243–53.
- [21] Boone CD, Bernath PF. Tangent height determination from the N₂ continuum for the Atmospheric Chemistry Experiment Fourier transform spectrometer. *J Quant Spectrosc Radiat Transf* 2019;238:106481.
- [22] Bernath PF, Boone CD, Fernando A, Jones S. Low altitude CO₂ from the Atmospheric Chemistry Experiment (ACE) satellite. *J Quant Spectrosc Radiat Transf* 2019;238:106528.
- [23] Zasetsky AY, Gilbert K, Galkina I, McLeod S, Sloan JJ. Properties of polar stratospheric clouds obtained by combined ACE-FTS and ACE-Imager extinction measurements. *Atmos Chem Phys Discuss* 2007;7:13271–90.
- [24] <https://mark4sun.jpl.nasa.gov/pseudo.html>.
- [25] Boone CD, Walker KA, Bernath PF. Speed-dependent Voigt profile for water vapor in infrared remote sensing applications. *J Quant Spectrosc Radiat Transf* 2007;105:525–32.
- [26] Ngo NH, Tran H, Gamache RR, Hartmann J-M. Pressure effects on water vapour lines: beyond the Voigt profile. *Philos Trans R Soc A* 2012;370:2495–508.
- [27] Boone CD, Walker KA, Bernath PF. An efficient analytical approach for calculating line mixing in atmospheric remote sensing applications. *J Quant Spectrosc Radiat Transf* 2011;112:980–9.
- [28] Rosenkranz PW. Shape of the 5 mm oxygen band in the atmosphere. *IEEE Trans Antennas Propag* 1975;AP-23:498–506.
- [29] Tran H, Ngo NH, Hartmann J-M. Efficient computation of some speed-dependent isolated line profiles. *J Quant Spectrosc Radiat Transf* 2013;129:199–203.
- [30] Hartmann J-M, Tran H. Note on the two possible formulations of the Hartmann-Tran line profile. *J Quant Spectrosc Radiat Transf* 2019;233:76–7.
- [31] Tran H, Ngo NH, Hartmann J-M. Erratum to “Efficient computation of some speed-dependent isolated line profiles”. [*J. Quant. Spectrosc. Radiat. Transfer* 129 (2013) 199–203]. *J Quant Spectrosc Radiat Transf* 2014;134:104.
- [32] Cousin C, Doucen RL, Boulet C, Henry A. Temperature dependence of the absorption in the region beyond the 4.3-μm band head of CO₂: N₂ and O₂ broadening. *Appl Opt* 1985;24(22):3899–907.
- [33] Toon GC, Wunch D. A stand-alone a priori profile generation tool for GGG2014 release. Caltech data; 2017. doi:10.14291/tcon.ggg2014.priors.r0/1221661.
- [34] Dufour G, Szopa S, Harrison JJ, Boone CD, Bernath PF. Seasonal variations of acetone in the upper troposphere-lower stratosphere of the northern midlatitudes as observed by ACE-FTS. *J Mol Spectrosc* 2016;323:67–77.
- [35] Manney GL, Santee ML, Rex M, Livesey NL, Pitts MC, Veefkind P, et al. Unprecedented Arctic ozone loss in 2011. *Nature* 2011;478:469–75.
- [36] Rollins AW, Thornberry TD, Watts LA, Yu P, Rosenlof KH, Mills M, et al. The role of sulfur dioxide in stratospheric aerosol formation evaluated by using in situ measurements in the tropical lower stratosphere. *Geophys Res Lett* 2017;44:4280–6.